

Logarithmic electroweak corrections to gauge-boson pair production at the LHC

E. ACCOMANDO¹, A. DENNER² AND A. KAISER^{2,3}

¹ *Dipartimento di Fisica Teorica, Università di Torino,
Via P. Giuria 1, 10125 Torino, Italy*

² *Paul Scherrer Institut
CH-5232 Villigen PSI, Switzerland*

³ *Institute of Theoretical Physics
University of Zürich, CH-8057 Zürich, Switzerland*

Abstract:

We have studied the effects of the complete logarithmic electroweak $\mathcal{O}(\alpha)$ corrections on the production of vector-boson pairs WZ, ZZ, and WW at the LHC. These corrections are implemented into a Monte Carlo program for $pp \rightarrow 4f(+\gamma)$ with final states involving four or two leptons using the double-pole approximation. We numerically investigate purely leptonic final states and find that electroweak corrections lower the predictions by 5–30% in the physically interesting region of large di-boson invariant mass and large angle of the produced vector bosons.

September 2004

1 Introduction

The production of gauge-boson pairs provides an excellent opportunity to test the non-abelian structure of the Standard Model (SM). Gauge-boson-pair-production amplitudes involve trilinear gauge-boson couplings. Therefore, the corresponding cross sections depend very sensitively on the non-abelian structure of the underlying theory. For this reason, vector-boson pair production has found continuous interest in the literature. In the last few years, gauge-boson self-interactions were directly measured at LEP2 and Tevatron. Still, up to now these couplings have not been determined with the same precision as other boson properties, such as their masses and couplings to fermions. Despite of the high statistics reached at LEP2 in producing W^+W^- pairs, the resulting limits on possible anomalous couplings, which parametrize deviations from SM predictions due to new physics occurring at energy scales of order of tens of TeV, are not very stringent. The weakness of the LEP2 measurement is the rather modest centre-of-mass (CM) energy of the produced W-boson pairs. On the other hand, anomalous gauge-boson couplings cause strong enhancements in the gauge-boson-pair-production cross section especially at large values of the di-boson invariant mass $M_{VV'}$ ($V, V' = W, Z$). A significant improvement in the bounds on triple-gauge-boson couplings is expected from measurements at future colliders operating at high energies such as the Large Hadron Collider (LHC). Therefore, in order to achieve a better precision in the determination of these couplings, it will be useful to analyse di-boson production at hadron colliders at the highest possible CM energies.

Vector-boson pairs also constitute a background to other kinds of new-physics searches. One of the gold-plated signals for supersymmetry at hadron colliders is chargino-neutralino pair production, which would give rise to final states with three charged leptons and missing transverse momentum; the primary background to this signature is given by WZ production. Also final states coming from ZZ production could fake that supersymmetry signature if one of the leptons is lost in the beam pipe. Finally, $W^\pm W^\mp$ can dirty the measurements of chargino and slepton pair production, which both give rise to two leptons and missing energy. Leptonic final states, coming from $pp \rightarrow VV'$ ($V, V' = W, Z$), could also fake ZZ, WZ, and WW vector-boson scattering signals which are again expected to be enhanced at high CM energies.

In the near future, the LHC will be the main source of vector-boson pairs with large invariant mass $M_{VV'}$. The machine will collect thousands of events, the exact statistics depending on the particular process and luminosity [1]. With LHC approaching its goal of an integrated luminosity of 100 fb^{-1} , a large data sample will be available to start a detailed investigation of the trilinear vertices.

In order to match the experimental precision, theoretical predictions need to have an accuracy of the order of a few per cent to allow for a decent analysis of the data. At lowest order, this demands taking into account all spin correlations and finite-width effects. The easiest way to fulfil this requirement is to go beyond the *production* \times *decay* approach by computing the full processes $pp \rightarrow 4f$. The next step consists in a full understanding and control of higher-order QCD and electroweak (EW) corrections. In the past years, a large effort has gone into accurate calculations of hadronic di-boson production (for a review on the subject see Ref. [1]). The $\mathcal{O}(\alpha_s)$ QCD corrections to massive gauge-boson pair production and decay have been extensively analysed by many authors [2, 3, 4, 5, 6, 7, 8].

Several NLO Monte Carlo programs have been constructed and cross checked so that complete $\mathcal{O}(\alpha_s)$ corrections are now available [7, 8]. QCD corrections turn out to be quite significant at LHC energies. They can increase the lowest-order cross section by a factor of two if no cuts are applied and by one order of magnitude for large transverse momentum or large invariant mass of the vector bosons [2, 3]. By including a jet veto, their effects can be drastically reduced to the order of tens of per cent [6, 7], but in any case they have to be considered to get realistic and reliable estimates of total cross sections and distributions.

In view of the envisaged precision of a few per cent at the LHC, also a discussion of EW corrections is in order. For single W- and Z-boson production, $\mathcal{O}(\alpha)$ corrections have been computed taking into account the full electromagnetic and weak contributions [9]. One-loop weak corrections have been also investigated for $t\bar{t}$ production [10], $b\bar{b}$ production [11], $\gamma/Z + \text{jet}$ hadro-production [12], WH and ZH production [13], as well as for γZ production [14]. By contrast, gauge-boson pair production at hadron colliders is commonly treated by including only universal radiative corrections such as the running of the electromagnetic coupling, and corrections to the ρ parameter. This approach is based on the belief that the remaining EW corrections (dominated by double-logarithmic contributions) are not relevant at the LHC just because physical cross sections decrease strongly with increasing invariant mass of the gauge-boson pairs, i.e. where EW corrections can be non-negligible. However, a first analysis of the effect of one-loop logarithmic EW corrections on WZ and $W\gamma$ production processes at the LHC [15] has instead demonstrated that $\mathcal{O}(\alpha)$ corrections are of the same order or bigger than the statistical error, when exploring the large di-boson invariant-mass and small rapidity region.

The fact that $\mathcal{O}(\alpha)$ EW corrections grow with increasing energy is well known since long time. EW corrections are in fact dominated by double and single logarithms of the ratio of the energy to the EW scale. Analyses of the general high-energy behaviour of EW corrections have been extensively performed (see for instance Refs. [16, 17]). A process-independent recipe for the calculation of logarithmic EW corrections is given in Refs. [18, 19, 20], where it has been shown that the logarithmic one-loop corrections to arbitrary EW processes factorize into tree-level amplitudes times universal correction factors.

Using the method of Refs. [18, 19, 20], we investigate in this paper the effect of logarithmic EW corrections to the hadronic production of $W^\pm Z$, ZZ , and $W^\pm W^\mp$ pairs in the large-invariant-mass region of the hard process at the LHC. Going beyond the analysis of Ref. [15], which addressed only logarithmic contributions originating from above the EW scale, here we consider also the effect of the complete logarithmic electromagnetic corrections. Since the aim of the paper is to analyse the structure of the $\mathcal{O}(\alpha)$ EW corrections and to give an estimate of their size, we have not included QCD corrections.

The simplest experimental analyses of gauge-boson pair production will rely on purely leptonic final states. Semi-leptonic channels, where one of the vector bosons decays hadronically, have been analysed at the Tevatron [21] showing that these events suffer from the background due to the production of one vector boson plus jets via gluon exchange. For this reason, we study only di-boson production where both gauge bosons decay leptonically into e or μ .

The paper is organized as follows: the strategy of our calculation is presented in Sect. 2. In Sect. 3 we describe the calculation of the lowest-order matrix elements, and in Sect. 4 the analytical results for the virtual logarithmic EW one-loop corrections are summarized. The treatment of soft and collinear singularities is discussed in Sect. 5. While the general setup of our numerical calculation is given in Sect. 6, Sect. 7 contains a numerical discussion for processes mediated by WZ, ZZ, and WW production. Our findings are summarized in Sect. 8. Appendices A and B contain results for non-factorizable corrections to a general class of processes and the corresponding integrals. Some coupling factors are listed in Appendix C.

2 Strategy of the calculation

We consider the production of massive gauge-boson pairs in hadron-hadron collisions. The generic process can be written as

$$h_1 + h_2 \rightarrow V_1 + V_2 + X \rightarrow f_3 + \bar{f}_4 + f_5 + \bar{f}_6 + X, \quad (2.1)$$

where h_1 and h_2 denote the incoming hadrons, V_1 and V_2 two arbitrary massive gauge bosons, e.g. W or Z bosons, f_3, f_5 the outgoing fermions, \bar{f}_4, \bar{f}_6 the outgoing antifermions, and X the remnants of the hadrons.

In the parton model the corresponding cross sections are obtained from a convolution as

$$d\sigma^{h_1 h_2}(P_1, P_2, p_f) = \sum_{i,j} \int_0^1 dx_1 \int_0^1 dx_2 \Phi_{i,h_1}(x_1, Q^2) \Phi_{j,h_2}(x_2, Q^2) d\hat{\sigma}^{ij}(x_1 P_1, x_2 P_2, p_f), \quad (2.2)$$

where p_f summarizes the final-state momenta, Φ_{i,h_1} and Φ_{j,h_2} are the distribution functions of the partons i and j in the incoming hadrons h_1 and h_2 with momenta P_1 and P_2 , respectively, Q is the factorization scale, and $d\hat{\sigma}^{ij}$ represent the differential cross sections for the partonic processes averaged over colours and spins of the partons. The sum $\sum_{i,j}$ runs over all possible quarks and antiquarks of flavour u, d, c, and s.

The relevant parton processes are of the form

$$\begin{aligned} \bar{q}_1(p_1, \sigma_1) + q_2(p_2, \sigma_2) &\rightarrow V_1(k_1, \lambda_1) + V_2(k_2, \lambda_2) \\ &\rightarrow f_3(p_3, \sigma_3) + \bar{f}_4(p_4, \sigma_4) + f_5(p_5, \sigma_5) + \bar{f}_6(p_6, \sigma_6). \end{aligned} \quad (2.3)$$

The arguments label the momenta p_i, k_l and helicities $\sigma_i = \pm 1/2, \lambda_l = 0, \pm 1$ of the corresponding incoming partons, outgoing fermions, and virtual gauge bosons. We often use only the signs to denote the helicities. The momenta of the incoming partons are related to the momenta of the hadrons by $p_1 = x_1 P_1$ and $p_2 = x_2 P_2$ if i is an antiquark and j a quark and by $p_2 = x_1 P_1$ and $p_1 = x_2 P_2$ in the opposite case.

The corresponding lowest-order partonic cross sections are calculated using the complete matrix elements. This means that we include the full set of Feynman diagrams, in this way accounting for all irreducible background coming from non-doubly resonant contributions. The calculation of the matrix elements for the complete process

$$\bar{q}_1(p_1, \sigma_1) + q_2(p_2, \sigma_2) \rightarrow f_3(p_3, \sigma_3) + \bar{f}_4(p_4, \sigma_4) + f_5(p_5, \sigma_5) + \bar{f}_6(p_6, \sigma_6) \quad (2.4)$$

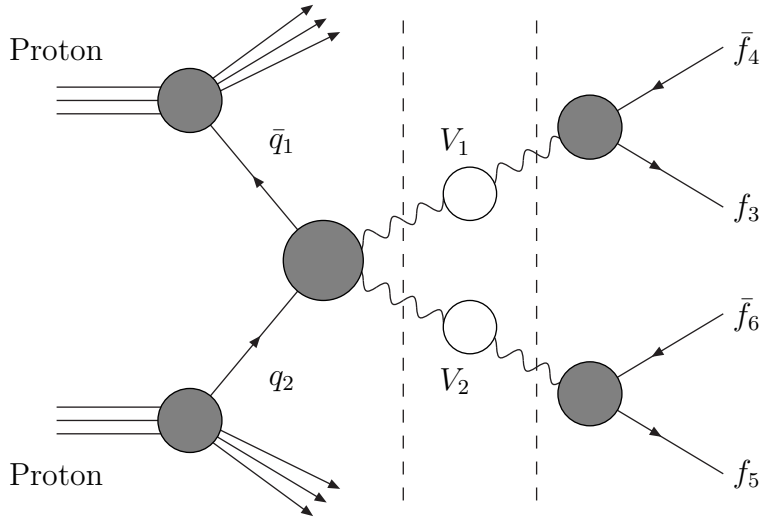


Figure 1: Structure of the process $pp \rightarrow V_1V_2 + X \rightarrow 4f + X$

is described in Sect. 3.

The electroweak radiative corrections to (2.4) consist of virtual corrections, resulting from loop diagrams, as well as of real corrections, originating from the processes

$$\bar{q}_1(p_1, \sigma_1) + q_2(p_2, \sigma_2) \rightarrow f_3(p_3, \sigma_3) + \bar{f}_4(p_4, \sigma_4) + f_5(p_5, \sigma_5) + \bar{f}_6(p_6, \sigma_6) + \gamma(k, \lambda_\gamma) \quad (2.5)$$

with an additional photon with momentum k and helicity $\lambda_\gamma = \pm 1$. Both have to be combined properly in order to ensure the cancellations of soft and collinear singularities (cf. Sect. 5).

For the calculation of the radiative corrections we follow the approach used for the process $e^+e^- \rightarrow W^+W^- \rightarrow 4f$ in Ref. [22]. The virtual corrections are calculated in the double-pole approximation (DPA), i.e. we take only those terms into account that are enhanced by two resonant massive gauge-boson propagators. The real corrections are calculated from the full matrix elements for the processes (2.5).

2.1 Double-pole approximation for virtual corrections

In DPA the processes $\bar{q}_1q_2 \rightarrow V_1V_2 \rightarrow 4f$ are divided into the production of on-shell gauge bosons and their decay into fermion–antifermion pairs (see Fig. 1).

At tree level, the matrix elements in DPA for the partonic processes $\bar{q}_1q_2 \rightarrow V_1V_2 \rightarrow 4f$ factorize into those for the production of two on-shell bosons, $\mathcal{M}_{\text{Born}}^{\bar{q}_1q_2 \rightarrow V_{1,\lambda_1}V_{2,\lambda_2}}$, the propagators of these bosons, and the matrix elements for their on-shell decays, $\mathcal{M}_{\text{Born}}^{V_{1,\lambda_1} \rightarrow f_3\bar{f}_4}$ and $\mathcal{M}_{\text{Born}}^{V_{2,\lambda_2} \rightarrow f_5\bar{f}_6}$,

$$\mathcal{M}_{\text{Born,DPA}}^{\bar{q}_1q_2 \rightarrow V_1V_2 \rightarrow 4f} = P_{V_1}(k_1^2) P_{V_2}(k_2^2) \sum_{\lambda_1, \lambda_2} \mathcal{M}_{\text{Born}}^{\bar{q}_1q_2 \rightarrow V_{1,\lambda_1}V_{2,\lambda_2}} \mathcal{M}_{\text{Born}}^{V_{1,\lambda_1} \rightarrow f_3\bar{f}_4} \mathcal{M}_{\text{Born}}^{V_{2,\lambda_2} \rightarrow f_5\bar{f}_6}. \quad (2.6)$$

The sum runs over the physical helicities $\lambda_1, \lambda_2 = 0, \pm 1$ of the on-shell projected gauge bosons V_1 and V_2 with momenta k_1 and k_2 , respectively. The propagators of the massive gauge bosons

$$P_V(p^2) = \frac{1}{p^2 - M_V^2 + \theta(p^2)iM_V\Gamma_V}, \quad V = W, Z, \quad (2.7)$$

involve besides the masses of the gauge bosons also their widths, which we consider as constant and finite for time-like momenta. The on-shell matrix elements are calculated using on-shell projected momenta as defined in Appendix A of Ref. [22]. Of course, the momenta in the resonant propagators are not projected on shell.

In DPA there are two types of corrections, factorizable and non-factorizable ones. The former are those that can be associated to one of the production or decay subprocesses, the latter are those that connect these subprocesses.

The factorizable corrections can be expressed in terms of the corrections to the on-shell gauge-boson-pair-production and -decay subprocesses. The matrix elements for the virtual factorizable corrections to the processes $\bar{q}_1 q_2 \rightarrow V_1 V_2 \rightarrow 4f$ can be written as

$$\begin{aligned} \delta\mathcal{M}_{\text{virt,DPA,fact}}^{\bar{q}_1 q_2 \rightarrow V_1 V_2 \rightarrow 4f} &= P_{V_1}(k_1^2) P_{V_2}(k_2^2) \sum_{\lambda_1, \lambda_2} \left\{ \delta\mathcal{M}_{\text{virt}}^{\bar{q}_1 q_2 \rightarrow V_{1,\lambda_1} V_{2,\lambda_2}} \mathcal{M}_{\text{Born}}^{V_{1,\lambda_1} \rightarrow f_3 \bar{f}_4} \mathcal{M}_{\text{Born}}^{V_{2,\lambda_2} \rightarrow f_5 \bar{f}_6} \right. \\ &\quad + \mathcal{M}_{\text{Born}}^{\bar{q}_1 q_2 \rightarrow V_{1,\lambda_1} V_{2,\lambda_2}} \delta\mathcal{M}_{\text{virt}}^{V_{1,\lambda_1} \rightarrow f_3 \bar{f}_4} \mathcal{M}_{\text{Born}}^{V_{2,\lambda_2} \rightarrow f_5 \bar{f}_6} \\ &\quad \left. + \mathcal{M}_{\text{Born}}^{\bar{q}_1 q_2 \rightarrow V_{1,\lambda_1} V_{2,\lambda_2}} \mathcal{M}_{\text{Born}}^{V_{1,\lambda_1} \rightarrow f_3 \bar{f}_4} \delta\mathcal{M}_{\text{virt}}^{V_{2,\lambda_2} \rightarrow f_5 \bar{f}_6} \right\}, \end{aligned} \quad (2.8)$$

where $\delta\mathcal{M}_{\text{virt}}^{\bar{q}_1 q_2 \rightarrow V_{1,\lambda_1} V_{2,\lambda_2}}$, $\delta\mathcal{M}_{\text{virt}}^{V_{1,\lambda_1} \rightarrow f_3 \bar{f}_4}$, and $\delta\mathcal{M}_{\text{virt}}^{V_{2,\lambda_2} \rightarrow f_5 \bar{f}_6}$ denote the virtual corrections to the on-shell matrix elements for the gauge-boson production and decay processes.

The non-factorizable corrections yield a simple correction factor $\delta_{\text{nf,DPA}}^{\text{virt}}$ to the lowest-order cross section. Its explicit form is given in Sect. 4.3.

The contribution of the complete virtual corrections in DPA to the cross section reads

$$\begin{aligned} \int d\sigma_{\text{virt,DPA}}^{\bar{q}_1 q_2 \rightarrow V_1 V_2 \rightarrow 4f} &= \frac{1}{2\hat{s}} \int d\Phi_{4f} \left[2 \text{Re} \left(\left(\mathcal{M}_{\text{Born,DPA}}^{\bar{q}_1 q_2 \rightarrow V_1 V_2 \rightarrow 4f} \right)^* \delta\mathcal{M}_{\text{virt,DPA,fact}}^{\bar{q}_1 q_2 \rightarrow V_1 V_2 \rightarrow 4f} \right) \right. \\ &\quad \left. + \left| \mathcal{M}_{\text{Born,DPA}}^{\bar{q}_1 q_2 \rightarrow V_1 V_2 \rightarrow 4f} \right|^2 \delta_{\text{nf,DPA}}^{\text{virt}} \right], \end{aligned} \quad (2.9)$$

where $d\Phi_{4f}$ denotes the four-particle phase-space element and $\hat{s} = (p_1 + p_2)^2$ the square of the CM energy in the partonic system. For some four-fermion final states resonant massive gauge bosons can either be formed from the pairs (f_3, \bar{f}_4) and (f_5, \bar{f}_6) or from the pairs (f_3, \bar{f}_6) and (f_5, \bar{f}_4) . Denoting the isospin partner of f by f' , this is the case for $f_3 = f_4 = f_5 = f_6$ and $f_3 = f_4 = f_5 = f'_6$, which allow for two different sets of ZZ and WZ pairs, respectively. In all these cases a DPA has to be defined for each of the two sets of resonant gauge bosons separately, and the cross sections from these two cases have to be summed.¹

¹In our numerical calculation we actually do not add the cross sections but the matrix elements for the different resonant sets. Since the interference between these different contributions is non-doubly resonant, this is equivalent within DPA accuracy.

Finally, we have to take care of the proper matching of the infrared (IR) and collinear singularities. In general the total cross section is composed as

$$\int d\sigma = \int_{\Phi_{4f}} d\sigma_{\text{Born}}^{\bar{q}_1 q_2 \rightarrow 4f} + \int_{\Phi_{4f}} d\sigma_{\text{virt}}^{\bar{q}_1 q_2 \rightarrow 4f} + \int_{\Phi_{4f\gamma}} d\sigma^{\bar{q}_1 q_2 \rightarrow 4f\gamma}. \quad (2.10)$$

Here $d\sigma_{\text{Born}}^{\bar{q}_1 q_2 \rightarrow 4f}$ is the full differential lowest-order cross section for $\bar{q}_1 q_2 \rightarrow 4f$ that is to be integrated over the four-particle phase space Φ_{4f} , i.e.

$$d\sigma_{\text{Born}}^{\bar{q}_1 q_2 \rightarrow 4f} = \frac{1}{2\hat{s}} \left| \mathcal{M}_{\text{Born}}^{\bar{q}_1 q_2 \rightarrow 4f} \right|^2 d\Phi_{4f}. \quad (2.11)$$

Similarly, $d\sigma^{\bar{q}_1 q_2 \rightarrow 4f\gamma}$, which describes the real corrections, is the full lowest-order cross section for $\bar{q}_1 q_2 \rightarrow 4f\gamma$ to be integrated over the five-particle phase space $\Phi_{4f\gamma}$, and $d\sigma_{\text{virt}}^{\bar{q}_1 q_2 \rightarrow 4f}$ denotes the virtual one-loop corrections.

Both $d\sigma^{\bar{q}_1 q_2 \rightarrow 4f\gamma}$ and $d\sigma_{\text{virt}}^{\bar{q}_1 q_2 \rightarrow 4f}$ involve soft and collinear singularities that cancel in their sum. Taking the DPA for $d\sigma_{\text{virt}}^{\bar{q}_1 q_2 \rightarrow 4f}$ but not for $d\sigma^{\bar{q}_1 q_2 \rightarrow 4f\gamma}$ spoils this cancellation. Therefore, we subtract the singular contributions $d\sigma_{\text{virt,sing}}^{\bar{q}_1 q_2 \rightarrow 4f}$ before we impose the DPA and replace (2.10) by

$$\begin{aligned} \int d\sigma &= \int_{\Phi_{4f}} d\sigma_{\text{Born}}^{\bar{q}_1 q_2 \rightarrow 4f} + \int_{\Phi_{4f}} (d\sigma_{\text{virt,DPA}}^{\bar{q}_1 q_2 \rightarrow 4f} - d\sigma_{\text{virt,sing,DPA}}^{\bar{q}_1 q_2 \rightarrow 4f}) \\ &\quad + \int_{\Phi_{4f}} d\sigma_{\text{virt,sing}}^{\bar{q}_1 q_2 \rightarrow 4f} + \int_{\Phi_{4f\gamma}} d\sigma^{\bar{q}_1 q_2 \rightarrow 4f\gamma}. \end{aligned} \quad (2.12)$$

Since the finite, non-logarithmic terms of $d\sigma_{\text{virt,sing}}^{\bar{q}_1 q_2 \rightarrow 4f}$ are not uniquely defined, this procedure leads to an ambiguity, which is, however, of the order of the uncertainty of the DPA. Since the IR- and fermion-mass-singular part is not treated in DPA, the logarithmic photonic corrections are not affected by this ambiguity. We use the definition of $d\sigma_{\text{virt,sing}}^{\bar{q}_1 q_2 \rightarrow 4f}$ as given in Sect. 5.2.

2.2 High-energy approximation

In contrast to Ref. [22], we do not calculate the EW $\mathcal{O}(\alpha)$ corrections completely, but we only calculate the logarithmic corrections in the high-energy limit. To this end, we consider the limit where all kinematical invariants $s_{ij} = (p_i + p_j)^2$ are large compared with the weak-boson mass scale, $|s_{ij}| \gg M_W^2$, and take into account all contributions proportional to $\alpha \ln^2(|s_{ij}|/M_W^2)$ or $\alpha \ln(|s_{ij}|/M_W^2)$. Note that this approximation is not applicable to the full processes $\bar{q}_1 q_2 \rightarrow V_1 V_2 \rightarrow 4f$ because of the presence of the resonances with invariant masses of the order of M_W . But it is perfectly applicable to the subprocesses $\bar{q}_1 q_2 \rightarrow V_1 V_2$, $V_1 \rightarrow f_3 \bar{f}_4$, and $V_2 \rightarrow f_5 \bar{f}_6$ appearing in the DPA.

Since we assume that all kinematical invariants are of the same order of magnitude, we can write all large energy-dependent EW logarithms in terms of $\ln(\hat{s}/M_W^2)$, where \hat{s} is the CM energy squared of the partonic process. In Ref. [15] we have taken into account all contributions involving logarithms of the form $\ln(\hat{s}/M_W^2)$. These arise from scales larger than M_W and can be written in an $\text{SU}(2) \times \text{U}(1)$ symmetric form. We did not include logarithmic corrections of purely electromagnetic origin arising from scales smaller

than M_W . These involve logarithms of the form $\ln(M_W^2/m_f^2)$ or $\ln(M_W^2/\lambda^2)$, where λ is the photon mass regulator. In the present paper all large logarithms of electromagnetic origin are included as well. Since the decay processes involve no large-energy variable, the corresponding virtual corrections involve no large EW logarithms. However, they give rise to large electromagnetic logarithms.

In the high-energy approximation we omit all mass-suppressed terms, i.e. terms of order M_W^2/\hat{s} . Therefore we can omit the channels with one longitudinal and one transverse gauge boson that are mass suppressed for the di-boson production processes $\bar{q}_1 q_2 \rightarrow V_1 V_2 \rightarrow 4f$ and take into account only the corrections to the dominating channels involving two transverse (TT) or two longitudinal (LL) gauge bosons. On the other hand, we take into account the exact kinematics by evaluating the complete four-fermion phase space and use the exact values of the kinematical invariants in all formulas.

The logarithmic virtual EW corrections to the dominating channels of $\bar{q}_1 q_2 \rightarrow V_1 V_2$ are calculated using the general results for a high-energy approximation given in Refs. [18, 19, 20]. The validity of these results relies on the assumption that all kinematical variables \hat{s} , $|\hat{t}|$, and $|\hat{u}|$ are large compared with M_W^2 and approximately of the same size,

$$\hat{s} \sim |\hat{t}| \sim |\hat{u}| \gg M_W^2. \quad (2.13)$$

This implies that the produced gauge bosons have to be emitted at sufficiently large angles with respect to the beam. Hence, the validity range of the high-energy logarithmic approximation for the radiative corrections corresponds to the central region of the boson scattering angle in the di-boson rest frame. The t -channel pole in the Born matrix element gives rise to additional enhanced logarithms when integrated over the full kinematical range. Since these terms are not included in our $\mathcal{O}(\alpha)$ analysis, we have to take care that we do not get sizeable contributions from small scattering angles with respect to the beam. On the other hand, our formulas do not fake spurious contributions as long as $\hat{s}, |\hat{t}|, |\hat{u}| \gtrsim M_W^2$, since the large logarithms become small for $\hat{s}, |\hat{t}|, |\hat{u}| \sim M_W^2$.

The logarithmic approximation yields the dominant corrections for large kinematical invariants $|s_{ij}| \gg M_W^2$, but neglects finite, non-logarithmic, process-dependent $\mathcal{O}(\alpha)$ contributions. For $e^+e^- \rightarrow W^+W^-$, where complete $\mathcal{O}(\alpha)$ corrections and their high-energy limit are available [16], the latter turn out to be of order of a few per cent. We assume that this holds as well for similar processes like hadronic di-boson production. Neglecting non-logarithmic terms can therefore be considered a reasonable approximation at the LHC, where the experimental accuracy in the high-energy regime is at the few-per-cent level.

3 The matrix elements for $\bar{q}_1 q_2 \rightarrow 4f$

Our calculation involves two independent sets of matrix elements. The first set consists of the complete lowest-order matrix elements for the processes $\bar{q}_1 q_2 \rightarrow 4f$ and $\bar{q}_1 q_2 \rightarrow 4f\gamma$. This set is based on the generic matrix elements for $e^+e^- \rightarrow 4 \text{ fermions} + \gamma$ given in Ref. [23]. All Feynman diagrams contributing to a $2f \rightarrow 4f$ process can be constructed from only two fundamental topologies (see Fig. 2) by permuting the external particles f_a, \dots, f_f .

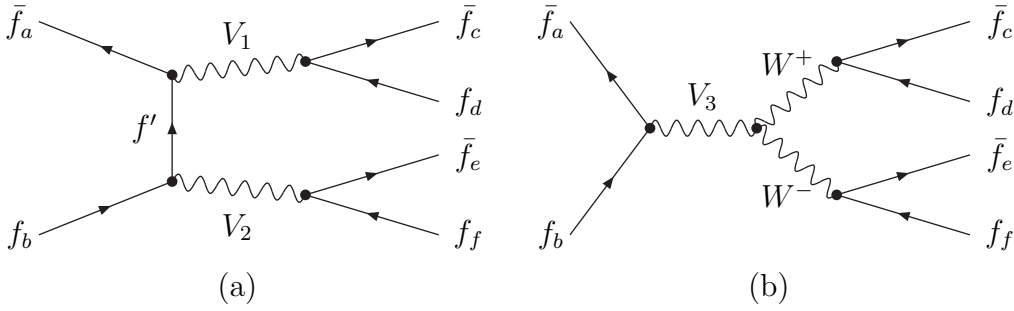


Figure 2: The fundamental topologies for processes with six external fermions

The second set of matrix elements is used for the calculation of the corrections in the DPA. It includes the matrix elements $\mathcal{M}^{\bar{q}_1 q_2 \rightarrow V_1 V_2}$ for the production of a pair of transverse or longitudinal gauge bosons and the matrix elements $\mathcal{M}^{V \rightarrow f \bar{f}'}$ for their decay.

3.1 Matrix elements for four-fermion production

We need the amplitudes for the parton processes (2.4) and (2.5). To this end we consider a generic process with three incoming antifermions $\bar{f}_1, \bar{f}_3, \bar{f}_5$ and three incoming fermions f_2, f_4, f_6 :

$$\bar{f}_1(p_1, \sigma_1) + f_2(p_2, \sigma_2) + \bar{f}_3(-p_3, -\sigma_3) + f_4(-p_4, -\sigma_4) + \bar{f}_5(-p_5, -\sigma_5) + f_6(-p_6, -\sigma_6) \rightarrow 0. \quad (3.1)$$

The arguments denote the (incoming) momenta and helicities of the incoming fermions and antifermions.

Each Feynman diagram for the process (3.1) corresponds to one of the two generic diagrams in Fig. 2. These generic diagrams are given by

$$\begin{aligned} \mathcal{M}^{a, V_1, V_2}(\bar{f}_a, f_b, \bar{f}_c, f_d, \bar{f}_e, f_f) &= -4e^4 \left(\sum_{f'} C_{V_1 \bar{f}_a f'}^{\sigma_a, \sigma'} C_{V_2 \bar{f}' f_b}^{-\sigma', \sigma_b} \right) C_{V_1 \bar{f}_c f_d}^{\sigma_c, \sigma_d} C_{V_2 \bar{f}_e f_f}^{\sigma_e, \sigma_f} \\ &\times \frac{P_{V_1}((p_c + p_d)^2) P_{V_2}((p_e + p_f)^2)}{(p_b + p_e + p_f)^2} A_2^{\sigma_a, \sigma_c, \sigma_e}(p_a, p_b, p_c, p_d, p_e, p_f), \\ \mathcal{M}^{b, V_3}(\bar{f}_a, f_b, \bar{f}_c, f_d, \bar{f}_e, f_f) &= -4e^4 C_{V_3 W^+ W^-} C_{V_3 \bar{f}_a f_b}^{\sigma_a, \sigma_b} C_{W^+ \bar{f}_c f_d}^{\sigma_c, \sigma_d} C_{W^- \bar{f}_e f_f}^{\sigma_e, \sigma_f} \\ &\times P_{V_3}((p_a + p_b)^2) P_{W^+}((p_c + p_d)^2) P_{W^-}((p_e + p_f)^2) A_3^{\sigma_a}(p_a, p_b, p_c, p_d, p_e, p_f), \end{aligned} \quad (3.2)$$

and the auxiliary functions A_2 and A_3 can be found in Ref. [23]. The gauge-boson propagators P_V are defined by (2.7), and e is the electric charge of the positron. For the photon ($V = A$), the Z boson, and the W boson, the generic couplings $C_{V \bar{f}_a f_b}^{\sigma_a, \sigma_b}$ are listed in (C.5) with (C.1). The coupling $C_{V_3 W^+ W^-}$ is given by

$$C_{AW^+ W^-} = 1, \quad C_{ZW^+ W^-} = -\frac{c_W}{s_W}. \quad (3.3)$$

where $c_w = M_W/M_Z$ and s_w are the cosine and sine of the electroweak mixing angle, respectively. If gluons are present, (3.2) corresponds to the matrix element with colour matrices omitted, and the generic fermionic couplings read

$$C_{gf_a f_b}^{\sigma_a, \sigma_b} = \delta_{\sigma_a, -\sigma_b} \frac{g_s}{e} \quad (3.4)$$

with the strong gauge coupling $g_s = \sqrt{4\pi\alpha_s}$. The matrix elements for outgoing particles are simply obtained by inverting the helicities and momenta. It is convenient to define the objects

$$\begin{aligned} \mathcal{M}_{\pm}^{\text{weak}} &= \sum_{\{i_1, i_3, i_5\}} \sum_{\{i_2, i_4, i_6\}} \frac{\text{sign}(\{i_1, i_3, i_5\}) \text{sign}(\{i_2, i_4, i_6\}) \pm 1}{2} \\ &\times \left[\sum_{V_1=W^\pm, Z, \gamma} \sum_{V_2=W^\pm, Z, \gamma} \mathcal{M}^{a, V_1, V_2}(\bar{f}_{i_1}, f_{i_2}, \bar{f}_{i_3}, f_{i_4}, \bar{f}_{i_5}, f_{i_6}) \right. \\ &\quad \left. + \sum_{V_3=Z, \gamma} \mathcal{M}^{b, V_3}(\bar{f}_{i_1}, f_{i_2}, \bar{f}_{i_3}, f_{i_4}, \bar{f}_{i_5}, f_{i_6}) \right] \quad (3.5) \end{aligned}$$

and

$$\begin{aligned} \mathcal{M}_{\pm}^{\text{gluon}} &= \sum_{\{i_1, i_3, i_5\}} \sum_{\{i_2, i_4, i_6\}} \frac{\text{sign}(\{i_1, i_3, i_5\}) \text{sign}(\{i_2, i_4, i_6\}) \pm 1}{2} \\ &\times \left[\sum_{V=W^\pm, Z, \gamma} \mathcal{M}^{a, g, V}(\bar{f}_{i_1}, f_{i_2}, \bar{f}_{i_3}, f_{i_4}, \bar{f}_{i_5}, f_{i_6}) \right. \\ &\quad \left. + \sum_{V=W^\pm, Z, \gamma} \mathcal{M}^{a, V, g}(\bar{f}_{i_1}, f_{i_2}, \bar{f}_{i_3}, f_{i_4}, \bar{f}_{i_5}, f_{i_6}) \right], \quad (3.6) \end{aligned}$$

where the two sums run over the permutations of the fermions and antifermions and $\text{sign}(\{i_1, i_3, i_5\})$ and $\text{sign}(\{i_2, i_4, i_6\})$ give the signs of these permutations. Note that $\mathcal{M}_+^{\text{weak}}$ is the sum of all diagrams with a positive signature of all permutations and $\mathcal{M}_-^{\text{weak}}$ is the sum of all diagrams with a negative signature. All diagrams that are not present in the SM, e.g. diagrams including a $Z\bar{u}e^-$ coupling or a $W^+d\bar{u}$ coupling, drop out because the corresponding values of the generic couplings vanish.

For a process that involves just one quark–antiquark pair, the matrix element squared and summed over colours and spins of the fermions and antifermions reads

$$|\mathcal{M}_{2 \text{ quarks}}|^2 = N_{\text{colour}} \sum_{\sigma_1, \dots, \sigma_6} |\mathcal{M}_+^{\text{weak}} + \mathcal{M}_-^{\text{weak}}|^2 \quad (3.7)$$

with the colour factor $N_{\text{colour}} = 3$. For a specific $2f \rightarrow 4f$ process this has to be divided by $4N_{\text{av}}N_{\text{sym}}$ in order to average over the polarizations and colours of the initial state and to take into account identical particles in the final state. For initial state quarks we have $N_{\text{av}} = 9$, and the symmetry factor is given by $N_{\text{sym}} = 2^{N_{\text{id}}}$ for N_{id} pairs of identical particles in the final state.

If there are four quarks, two additional complications must be taken into account. First the exchange of gluons between two pairs of quarks becomes possible giving rise to

additional Feynman diagrams with gluon exchange, and secondly we get different colour structures. For the squared matrix element with four quarks summed over polarizations and colours we find

$$\begin{aligned}
|\mathcal{M}_{4\text{quarks}}|^2 = & \sum_{\sigma_1, \dots, \sigma_6} \left[9 |\mathcal{M}_+^{\text{weak}}|^2 + 9 |\mathcal{M}_-^{\text{weak}}|^2 + 2 |\mathcal{M}_+^{\text{gluon}}|^2 + 2 |\mathcal{M}_-^{\text{gluon}}|^2 \right. \\
& + 6 \operatorname{Re} \left(\mathcal{M}_+^{\text{weak}} (\mathcal{M}_-^{\text{weak}})^* \right) + 8 \operatorname{Re} \left(\mathcal{M}_+^{\text{weak}} (\mathcal{M}_-^{\text{gluon}})^* \right) \\
& \left. + 8 \operatorname{Re} \left(\mathcal{M}_-^{\text{weak}} (\mathcal{M}_+^{\text{gluon}})^* \right) - \frac{4}{3} \operatorname{Re} \left(\mathcal{M}_+^{\text{gluon}} (\mathcal{M}_-^{\text{gluon}})^* \right) \right]. \quad (3.8)
\end{aligned}$$

We do not consider processes with six quarks.

The matrix elements for four-fermion-plus-photon production are constructed in complete analogy to the matrix elements for four-fermion production from the generic diagrams given in Ref. [23].

3.2 Matrix elements for $\bar{q}_1 q_2 \rightarrow V_1 V_2$ and $V \rightarrow f \bar{f}'$

In DPA, we need matrix elements for the processes

$$\begin{aligned}
\bar{q}_1(p_1, \sigma_1) + q_2(p_2, \sigma_2) & \rightarrow V_1(k_1, \lambda_1) + V_2(k_2, \lambda_2), \\
V_1(k_1, \lambda_1) & \rightarrow f_3(p_3, \sigma_3) + \bar{f}_4(p_4, \sigma_4), \\
V_2(k_2, \lambda_2) & \rightarrow f_5(p_5, \sigma_5) + \bar{f}_6(p_6, \sigma_6). \quad (3.9)
\end{aligned}$$

We take all pairs of massive gauge bosons, i.e. W^+W^- , $W^\pm Z$, and ZZ , into account. Owing to the mixing of the Z boson with the photon also matrix elements for $W^\pm \gamma$ and $Z \gamma$ production occur in the results for the logarithmic EW radiative corrections. The logarithmic corrections for matrix elements involving longitudinal gauge bosons are calculated with the Goldstone-boson equivalence theorem. As a consequence of the mixing of the would-be Goldstone bosons with the Higgs boson, also the matrix elements for the production of a gauge boson and a Higgs boson appear. All these matrix elements have been calculated with the Weyl-van der Waerden spinor formalism. The results can be found in Ref. [24].

4 Logarithmic EW corrections

In DPA, the $\mathcal{O}(\alpha)$ contributions consist of factorizable corrections to gauge-boson production and decay as well as non-factorizable corrections as summarized in (2.9). In the following we list these corrections in the high-energy approximation.

4.1 Corrections to gauge-boson production

In this section, we present the analytical formulas for the logarithmic EW corrections to the polarized partonic subprocesses

$$\bar{q}_1(p_1, \sigma_1) + q_2(p_2, \sigma_2) \rightarrow V_1(k_1, \lambda_1) + V_2(k_2, \lambda_2), \quad (4.1)$$

which can be derived from the general results given in Ref. [18]. The photon field is denoted by A . The Mandelstam variables read

$$\hat{s} = (p_1 + p_2)^2, \quad \hat{t} = (p_1 - k_1)^2, \quad \hat{u} = (p_1 - k_2)^2, \quad (4.2)$$

where the momenta of the initial and final states are incoming and outgoing, respectively.

The one-loop corrections are evaluated in the limit (2.13), and we neglect combinations of gauge-boson helicities that are mass-suppressed compared with $\sqrt{\hat{s}}$ in this limit. Thus, we do not consider corrections to the case of mixed longitudinal and transversely polarized gauge bosons. We calculate corrections to the non-suppressed purely longitudinal final state $(\lambda_1, \lambda_2) = (0, 0)$, which we denote by $(\lambda_1, \lambda_2) = (L, L)$, and to the purely transverse final states denoted by $(\lambda_1, \lambda_2) = (T, T)$, which includes the non-suppressed opposite-helicity final states $(\lambda_1, \lambda_2) = (\pm, \mp)$ and the suppressed equal-helicity final states $(\lambda_1, \lambda_2) = (\pm, \pm)$.

The leading and next-to-leading logarithms depend only on tree-level amplitudes and quantum numbers of the external particles, and thus are universal. Following Ref. [18], the logarithmic EW corrections can be written in the form

$$\delta\mathcal{M}^{\bar{q}_1 q_2 \rightarrow V_{1,\lambda_1} V_{2,\lambda_2}} = \delta^{\text{LSC}}\mathcal{M} + \delta^{\text{SSC}}\mathcal{M} + \delta^{\text{C}}\mathcal{M} + \delta^{\text{PR}}\mathcal{M}. \quad (4.3)$$

Here $\delta^{\text{LSC}}\mathcal{M}$ denotes the contribution of leading soft-collinear corrections and $\delta^{\text{SSC}}\mathcal{M}$ the contribution of the next-to-leading soft-collinear corrections, which are angular dependent. The term $\delta^{\text{C}}\mathcal{M}$ contains the collinear logarithms and the logarithms related to the renormalization of the incoming and outgoing fields. Finally, $\delta^{\text{PR}}\mathcal{M}$ are the logarithmic corrections that arise from parameter renormalization.

The following results are directly based on the formulas of Ref. [18] and written in a generic way for all processes $\bar{q}_1 q_2 \rightarrow V_1 V_2$. In this way they have been directly implemented in our Monte Carlo program. The amplitudes involving longitudinal gauge bosons are evaluated using the Goldstone-boson equivalence theorem. Therefore, it is convenient to write the results in terms of Born matrix elements with external would-be Goldstone bosons.² These matrix elements have to be understood as shorthands for matrix elements with external longitudinal gauge bosons according to

$$\begin{aligned} \mathcal{M}_{\text{Born}}^{\bar{q}_1 q_2 \rightarrow \Phi_1 \Phi_2} &= (-i)^{(Q_{V_1}+1)} (-i)^{(Q_{V_2}+1)} \mathcal{M}_{\text{Born}}^{\bar{q}_1 q_2 \rightarrow V_{1,L} V_{2,L}}, \\ \mathcal{M}_{\text{Born}}^{\bar{q}_1 q_2 \rightarrow H \Phi} &= (-i)^{(Q_V+1)} \mathcal{M}_{\text{Born}}^{\bar{q}_1 q_2 \rightarrow H V_L}, \end{aligned} \quad (4.4)$$

where Q_V are the charges of the outgoing gauge bosons.

4.1.1 Leading soft-collinear corrections

According to formulas (3.6) and (3.7) of Ref. [18], the leading soft-collinear corrections read

$$\begin{aligned} \delta^{\text{LSC}}\mathcal{M}^{\bar{q}_1 q_2 \rightarrow V_{1,T} V_{2,T}} &= \left(\delta_{\bar{q}_1 \bar{q}_1}^{\text{LSC}} + \delta_{q_2 q_2}^{\text{LSC}} + \delta_{V_1 V_1}^{\text{LSC}} + \delta_{V_2 V_2}^{\text{LSC}} \right) \mathcal{M}_{\text{Born}}^{\bar{q}_1 q_2 \rightarrow V_{1,T} V_{2,T}} \\ &\quad + \delta_{V_1 Z} \delta_{AV_1}^{\text{LSC}} \mathcal{M}_{\text{Born}}^{\bar{q}_1 q_2 \rightarrow AV_{2,T}} + \delta_{V_2 Z} \delta_{AV_2}^{\text{LSC}} \mathcal{M}_{\text{Born}}^{\bar{q}_1 q_2 \rightarrow V_{1,T} A} \end{aligned} \quad (4.5)$$

²We denote the would-be Goldstone bosons corresponding to the Z and W bosons by χ and ϕ , respectively.

for transverse gauge bosons and

$$\delta^{\text{LSC}} \mathcal{M}^{\bar{q}_1 q_2 \rightarrow V_{1,L} V_{2,L}} = \left(\delta_{\bar{q}_1 \bar{q}_1}^{\text{LSC}} + \delta_{q_2 q_2}^{\text{LSC}} + \delta_{\Phi_1 \Phi_1}^{\text{LSC}} + \delta_{\Phi_2 \Phi_2}^{\text{LSC}} \right) \mathcal{M}_{\text{Born}}^{\bar{q}_1 q_2 \rightarrow \Phi_1 \Phi_2} \quad (4.6)$$

for longitudinal gauge bosons, where Φ_1 and Φ_2 denote the would-be Goldstone bosons corresponding to $V_{1,L}$ and $V_{2,L}$, respectively. The factors $\delta_{\varphi' \varphi}^{\text{LSC}}$ are defined as

$$\delta_{\varphi' \varphi}^{\text{LSC}} = -\frac{\alpha}{8\pi} C_{\varphi' \varphi}^{\text{ew}} \ln^2 \left(\frac{\hat{s}}{M_W^2} \right) + \delta_{\varphi' \varphi} \left\{ \frac{\alpha}{4\pi} (I_\varphi^Z)^2 \ln \left(\frac{\hat{s}}{M_W^2} \right) \ln \left(\frac{M_Z^2}{M_W^2} \right) - \frac{1}{2} Q_\varphi^2 L^{\text{em}}(\hat{s}, \lambda^2, M_\varphi^2) \right\}, \quad (4.7)$$

where M_φ and Q_φ are the mass and relative charge, respectively, of the field $\varphi = q, \bar{q}, W^\pm, Z, \phi^\pm, \chi$, and λ is the photon mass regulator.

The term L^{em} contains all leading soft-collinear logarithms of pure electromagnetic origin:

$$L^{\text{em}}(\hat{s}, \lambda^2, M_\varphi^2) = \frac{\alpha}{4\pi} \left\{ 2 \ln \left(\frac{\hat{s}}{M_W^2} \right) \ln \left(\frac{M_W^2}{\lambda^2} \right) + \ln^2 \left(\frac{M_W^2}{\lambda^2} \right) - \ln^2 \left(\frac{M_\varphi^2}{\lambda^2} \right) \right\}. \quad (4.8)$$

The relevant non-vanishing components of the EW Casimir operator C^{ew} read

$$\begin{aligned} C_{qq}^{\text{ew}} = C_{\bar{q}\bar{q}}^{\text{ew}} &= \frac{(1 + 2c_w^2) + 4(Q_q^2 - 2I_q^3 Q_q) s_w^2}{4s_w^2 c_w^2}, \\ C_{\phi^\pm \phi^\pm}^{\text{ew}} = C_{\chi\chi}^{\text{ew}} &= \frac{1 + 2c_w^2}{4s_w^2 c_w^2}, \quad C_{W^\pm W^\pm}^{\text{ew}} = \frac{2}{s_w^2}, \\ C_{AA}^{\text{ew}} &= 2, \quad C_{AZ}^{\text{ew}} = C_{ZA}^{\text{ew}} = -2 \frac{c_w}{s_w}, \quad C_{ZZ}^{\text{ew}} = 2 \frac{c_w^2}{s_w^2}, \end{aligned} \quad (4.9)$$

and the relevant squared Z-boson couplings are given by

$$\begin{aligned} (I_q^Z)^2 &= (I_{\bar{q}}^Z)^2 = \frac{(Q_q s_w^2 - I_q^3)^2}{s_w^2 c_w^2}, \quad (I_W^Z)^2 = \frac{c_w^2}{s_w^2}, \\ (I_\phi^Z)^2 &= \frac{(c_w^2 - s_w^2)^2}{4s_w^2 c_w^2}, \quad (I_\chi^Z)^2 = \frac{1}{4s_w^2 c_w^2}. \end{aligned} \quad (4.10)$$

Finally, Q_q and I_q^3 denote the relative charge and the third component of the weak isospin of the quark q .

4.1.2 Subleading soft-collinear corrections

The angular-dependent subleading soft-collinear corrections are obtained from formula (3.12) of Ref. [18]. For the production of transverse gauge bosons we get

$$\begin{aligned} \delta_{\text{neutral}}^{\text{SSC}} \mathcal{M}^{\bar{q}_1 q_2 \rightarrow V_{1,T} V_{2,T}} &= \frac{\alpha}{2\pi} \sum_{V=A,Z} \left[\ln \left(\frac{\hat{s}}{M_W^2} \right) + \delta_{VA} \ln \left(\frac{M_W^2}{\lambda^2} \right) \right] \\ &\times \left\{ \ln \left(\frac{|\hat{t}|}{\hat{s}} \right) \left[I_{\bar{q}_1 \bar{q}_1}^{\bar{V}} I_{V_1 \bar{V}_1}^V + I_{q_2 q_2}^{\bar{V}} I_{V_2 \bar{V}_2}^V \right] \right. \\ &\left. + \ln \left(\frac{|\hat{u}|}{\hat{s}} \right) \left[I_{\bar{q}_1 \bar{q}_1}^{\bar{V}} I_{V_2 \bar{V}_2}^V + I_{q_2 q_2}^{\bar{V}} I_{V_1 \bar{V}_1}^V \right] \right\} \mathcal{M}_{\text{Born}}^{\bar{q}_1 q_2 \rightarrow V_{1,T} V_{2,T}} \end{aligned} \quad (4.11)$$

from the exchange of neutral virtual gauge bosons and

$$\begin{aligned}
\delta_{\text{charged}}^{\text{SSC}} \mathcal{M}^{\bar{q}_1 q_2 \rightarrow V_{1,T} V_{2,T}} &= \frac{\alpha}{2\pi} \sum_{V=W^\pm} \sum_{V'=A,Z,W^\pm} \sum_{q'} \ln \left(\frac{\hat{s}}{M_W^2} \right) \\
&\times \left\{ \ln \left(\frac{|\hat{t}|}{\hat{s}} \right) \left[I_{\bar{q}' \bar{q}_1}^{\bar{V}} I_{\bar{V}' \bar{V}_1}^V \mathcal{M}_{\text{Born}}^{\bar{q}' q_2 \rightarrow V_{1,T}' V_{2,T}} + I_{q' q_2}^{\bar{V}} I_{\bar{V}' \bar{V}_2}^V \mathcal{M}_{\text{Born}}^{\bar{q}_1 q' \rightarrow V_{1,T}' V_{2,T}'} \right] \right. \\
&\left. + \ln \left(\frac{|\hat{u}|}{\hat{s}} \right) \left[I_{\bar{q}' \bar{q}_1}^{\bar{V}} I_{\bar{V}' \bar{V}_2}^V \mathcal{M}_{\text{Born}}^{\bar{q}' q_2 \rightarrow V_{1,T}' V_{2,T}'} + I_{q' q_2}^{\bar{V}} I_{\bar{V}' \bar{V}_1}^V \mathcal{M}_{\text{Born}}^{\bar{q}_1 q' \rightarrow V_{1,T}' V_{2,T}'} \right] \right\} \quad (4.12)
\end{aligned}$$

from the exchange of charged virtual gauge bosons. The charge conjugated of the gauge boson V is denoted by \bar{V} . The couplings $I_{\bar{V}_2 \bar{V}_3}^{V_1}$ are defined in (C.3). The couplings $I_{q' q}^{\bar{V}}$, given in (C.1), involve the quark-mixing matrix, and quark mixing requires the sum over q' in (4.12). After using the unitarity of the quark-mixing matrix, the EW logarithmic corrections have exactly the same dependence on its matrix elements as the lowest order.

For the production of longitudinal gauge bosons we find

$$\begin{aligned}
\delta_{\text{neutral}}^{\text{SSC}} \mathcal{M}^{\bar{q}_1 q_2 \rightarrow V_{1,L} V_{2,L}} &= i^{((1+Q_{V_1})+(1+Q_{V_2}))} \delta_{\text{neutral}}^{\text{SSC}} \mathcal{M}^{\bar{q}_1 q_2 \rightarrow S_1 S_2} \\
&= i^{((1+Q_{V_1})+(1+Q_{V_2}))} \frac{\alpha}{2\pi} \sum_{V=A,Z} \sum_{S'=\chi,H,\phi^\pm} \left[\ln \left(\frac{\hat{s}}{M_W^2} \right) + \delta_{VA} \ln \left(\frac{M_W^2}{\lambda^2} \right) \right] \\
&\times \left\{ \ln \left(\frac{|\hat{t}|}{\hat{s}} \right) \left[I_{\bar{q}_1 \bar{q}_1}^{\bar{V}} I_{\bar{S}' \bar{S}_1}^V \mathcal{M}_{\text{Born}}^{\bar{q}_1 q_2 \rightarrow S' S_2} + I_{q_2 q_2}^{\bar{V}} I_{\bar{S}' \bar{S}_2}^V \mathcal{M}_{\text{Born}}^{\bar{q}_1 q_2 \rightarrow S_1 S'} \right] \right. \\
&\left. + \ln \left(\frac{|\hat{u}|}{\hat{s}} \right) \left[I_{\bar{q}_1 \bar{q}_1}^{\bar{V}} I_{\bar{S}' \bar{S}_2}^V \mathcal{M}_{\text{Born}}^{\bar{q}_1 q_2 \rightarrow S_1 S'} + I_{q_2 q_2}^{\bar{V}} I_{\bar{S}' \bar{S}_1}^V \mathcal{M}_{\text{Born}}^{\bar{q}_1 q_2 \rightarrow S' S_2} \right] \right\} \quad (4.13)
\end{aligned}$$

from the exchange of neutral virtual gauge bosons and

$$\begin{aligned}
\delta_{\text{charged}}^{\text{SSC}} \mathcal{M}^{\bar{q}_1 q_2 \rightarrow V_{1,L} V_{2,L}} &= i^{((1+Q_{V_1})+(1+Q_{V_2}))} \delta_{\text{charged}}^{\text{SSC}} \mathcal{M}^{\bar{q}_1 q_2 \rightarrow S_1 S_2} \\
&= i^{((1+Q_{V_1})+(1+Q_{V_2}))} \frac{\alpha}{2\pi} \sum_{V=W^\pm} \sum_{S'=\chi,H,\phi^\pm} \sum_{q'} \ln \left(\frac{\hat{s}}{M_W^2} \right) \\
&\times \left\{ \ln \left(\frac{|\hat{t}|}{\hat{s}} \right) \left[I_{\bar{q}' \bar{q}_1}^{\bar{V}} I_{\bar{S}' \bar{S}_1}^V \mathcal{M}_{\text{Born}}^{\bar{q}' q_2 \rightarrow S' S_2} + I_{q' q_2}^{\bar{V}} I_{\bar{S}' \bar{S}_2}^V \mathcal{M}_{\text{Born}}^{\bar{q}_1 q' \rightarrow S_1 S'} \right] \right. \\
&\left. + \ln \left(\frac{|\hat{u}|}{\hat{s}} \right) \left[I_{\bar{q}' \bar{q}_1}^{\bar{V}} I_{\bar{S}' \bar{S}_2}^V \mathcal{M}_{\text{Born}}^{\bar{q}' q_2 \rightarrow S_1 S'} + I_{q' q_2}^{\bar{V}} I_{\bar{S}' \bar{S}_1}^V \mathcal{M}_{\text{Born}}^{\bar{q}_1 q' \rightarrow S' S_2} \right] \right\} \quad (4.14)
\end{aligned}$$

from the exchange of charged virtual gauge bosons, where the couplings $I_{\bar{S}' \bar{S}_2}^V$ are defined in (C.4).

4.1.3 Collinear logarithms

The single collinear logarithms can be read off from formulas (4.2), (4.6), (4.10), (4.22), and (4.33) of Ref. [18]. Their contribution to the gauge-boson-production matrix element reads

$$\begin{aligned}
\delta^{\text{C}} \mathcal{M}^{\bar{q}_1 q_2 \rightarrow V_{1,T} V_{2,T}} &= \left(\delta_{\bar{q}_1 \bar{q}_1}^{\text{C}} + \delta_{q_2 q_2}^{\text{C}} + \delta_{V_{1,T} V_{1,T}}^{\text{C}} + \delta_{V_{2,T} V_{2,T}}^{\text{C}} \right) \mathcal{M}_{\text{Born}}^{\bar{q}_1 q_2 \rightarrow V_{1,T} V_{2,T}} \\
&+ \delta_{V_1 Z} \delta_{AV_{1,T}}^{\text{C}} \mathcal{M}_{\text{Born}}^{\bar{q}_1 q_2 \rightarrow AV_{2,T}} + \delta_{V_2 Z} \delta_{AV_{2,T}}^{\text{C}} \mathcal{M}_{\text{Born}}^{\bar{q}_1 q_2 \rightarrow V_{1,T} A} \quad (4.15)
\end{aligned}$$

in the case of transverse gauge bosons and

$$\delta^{\text{C}} \mathcal{M}^{\bar{q}_1 q_2 \rightarrow V_{1,L} V_{2,L}} = \left(\delta_{\bar{q}_1 \bar{q}_1}^{\text{C}} + \delta_{q_2 q_2}^{\text{C}} + \delta_{V_{1,L} V_{1,L}}^{\text{C}} + \delta_{V_{2,L} V_{2,L}}^{\text{C}} \right) \mathcal{M}_{\text{Born}}^{\bar{q}_1 q_2 \rightarrow V_{1,L} V_{2,L}} \quad (4.16)$$

in the case of longitudinal gauge bosons. The collinear correction factors for the different particles read

$$\begin{aligned} \delta_{q_\sigma q_\sigma}^{\text{C}} &= \delta_{\bar{q}_{-\sigma} \bar{q}_{-\sigma}}^{\text{C}} = \frac{\alpha}{4\pi} \left[\frac{3}{2} C_{q_\sigma q_\sigma}^{\text{ew}} \ln \left(\frac{\hat{s}}{M_W^2} \right) + Q_{q_\sigma}^2 \left(\frac{1}{2} \ln \left(\frac{M_W^2}{m_f^2} \right) + \ln \left(\frac{M_W^2}{\lambda^2} \right) \right) \right], \\ \delta_{W_T^\pm W_T^\pm}^{\text{C}} &= \frac{\alpha}{4\pi} \left[\frac{19}{12s_W^2} \ln \left(\frac{\hat{s}}{M_W^2} \right) + \ln \left(\frac{M_W^2}{\lambda^2} \right) \right], \\ \delta_{Z_T Z_T}^{\text{C}} &= \frac{\alpha}{4\pi} \frac{19 - 38s_W^2 - 22s_W^4}{12s_W^2 c_W^2} \ln \left(\frac{\hat{s}}{M_W^2} \right), \\ \delta_{AZ_T}^{\text{C}} &= -\frac{\alpha}{4\pi} \frac{19 + 22s_W^2}{6s_W c_W} \ln \left(\frac{\hat{s}}{M_W^2} \right), \\ \delta_{W_L^\pm W_L^\pm}^{\text{C}} &= \frac{\alpha}{4\pi} \left[\frac{1 + 2c_W^2}{2s_W^2 c_W^2} \ln \left(\frac{\hat{s}}{M_W^2} \right) - \frac{3}{4s_W^2} \frac{m_t^2}{M_W^2} \ln \left(\frac{\hat{s}}{m_t^2} \right) + \ln \left(\frac{M_W^2}{\lambda^2} \right) \right], \\ \delta_{Z_L Z_L}^{\text{C}} &= \frac{\alpha}{4\pi} \left[\frac{1 + 2c_W^2}{2s_W^2 c_W^2} \ln \left(\frac{\hat{s}}{M_W^2} \right) - \frac{3}{4s_W^2} \frac{m_t^2}{M_W^2} \ln \left(\frac{\hat{s}}{m_t^2} \right) \right]. \end{aligned} \quad (4.17)$$

While in Ref. [18] all masses of the order of the EW scale were replaced by M_W in the arguments of the large logarithms, we keep m_t in the logarithm resulting from top-quark loops.

4.1.4 Logarithms from parameter renormalization

The parameter renormalization gives rise to the so-called counter-term contributions which result from

$$\delta^{\text{PR}} \mathcal{M}^{\bar{q}_1 q_2 \rightarrow V_1 V_2} = \frac{\partial \mathcal{M}_{\text{Born}}^{\bar{q}_1 q_2 \rightarrow V_1 V_2}}{\partial e} \delta e + \frac{\partial \mathcal{M}_{\text{Born}}^{\bar{q}_1 q_2 \rightarrow V_1 V_2}}{\partial c_W} \delta c_W \Big|_{\mu^2 = \hat{s}}, \quad (4.18)$$

where δe and δc_W are the counter terms to the electric charge e and the cosine of the weak mixing angle $c_W = M_W/M_Z$, respectively. The mass parameter μ^2 of dimensional regularization is set to \hat{s} in order not to introduce spurious large logarithms. The counter terms depend on the explicit renormalization conditions. We fix them in the on-shell scheme and obtain in logarithmic approximation:

$$\frac{\delta e}{e} = \frac{1}{2} \left[\frac{\alpha}{4\pi} \frac{11}{3} \ln \left(\frac{\hat{s}}{M_W^2} \right) + \Delta\alpha(M_W^2) \right], \quad (4.19)$$

$$\frac{\delta c_W}{c_W} = -\frac{\alpha}{4\pi} \frac{19 + 22s_W^2}{12c_W^2} \ln \left(\frac{\hat{s}}{M_W^2} \right), \quad (4.20)$$

where

$$\Delta\alpha(M_W^2) = \frac{\alpha}{3\pi} \sum_{f \neq t} N_C^f Q_f^2 \ln \left(\frac{M_W^2}{m_f^2} \right) \quad (4.21)$$

describes the running of α from zero to the EW scale.

4.2 Corrections to gauge-boson decay

Since the decay matrix elements are independent of a large energy scale, no energy-dependent logarithms appear in the corresponding corrections. The only large logarithms result from electromagnetic corrections, i.e. from diagrams with photon exchange. For massless fermions these corrections turn out to be proportional to the lowest-order matrix element

$$\delta\mathcal{M}^{V\lambda\rightarrow f\bar{f}'} = \delta_{Vf\bar{f}'}\mathcal{M}_{\text{Born}}^{V\lambda\rightarrow f\bar{f}'}. \quad (4.22)$$

In the logarithmic approximation the correction factors for $V = Z$ and $V = W^\pm$ read

$$\begin{aligned} \delta_{Zf\bar{f}} &= \frac{\alpha}{4\pi}Q_f^2\left[\ln^2\frac{m_f^2}{\lambda^2} - \ln^2\frac{M_Z^2}{\lambda^2} + \ln\frac{M_Z^2}{m_f^2} + 2\ln\frac{M_Z^2}{\lambda^2}\right] + \frac{1}{2}\Delta\alpha(M_Z^2), \\ \delta_{Wf\bar{f}'} &= \frac{\alpha}{4\pi}\left\{\frac{1}{2}Q_f^2\left[\ln^2\frac{m_f^2}{\lambda^2} - \ln^2\frac{M_W^2}{\lambda^2} + \ln\frac{M_W^2}{m_f^2} + 2\ln\frac{M_W^2}{\lambda^2}\right] \right. \\ &\quad + \frac{1}{2}Q_{f'}^2\left[\ln^2\frac{m_{f'}^2}{\lambda^2} - \ln^2\frac{M_W^2}{\lambda^2} + \ln\frac{M_W^2}{m_{f'}^2} + 2\ln\frac{M_W^2}{\lambda^2}\right] \\ &\quad \left. + (Q_{f'} - Q_f)^2\ln\frac{M_W^2}{\lambda^2}\right\} + \frac{1}{2}\Delta\alpha(M_W^2). \end{aligned} \quad (4.23)$$

4.3 Non-factorizable corrections

The non-factorizable corrections for a general class of processes are evaluated in Appendix A. For the processes (2.4) the corresponding correction factor to the lowest-order cross section reads

$$\begin{aligned} \delta_{\text{nf,DPA}}^{\text{virt}} &= \frac{\alpha}{\pi}\left(-\sum_{i=3}^4\sum_{j=5}^6Q_iQ_j\theta_d(i)\theta_d(j)\text{Re}\{\Delta_1(k_1,p_i;k_2,p_j)\}\right. \\ &\quad + \sum_{k=1}^2\sum_{i=3}^4Q_kQ_i\theta_d(k)\theta_d(i)\text{Re}\{\Delta_2(p_k;k_1,p_i)\} \\ &\quad \left. + \sum_{k=1}^2\sum_{j=5}^6Q_kQ_j\theta_d(k)\theta_d(j)\text{Re}\{\Delta_2(p_k;k_2,p_j)\}\right) \end{aligned} \quad (4.24)$$

in DPA where Q_i are the relative charges of the fermions corresponding to the external legs and θ_d is defined by

$$\theta_d(i) = \begin{cases} +1 & \text{for incoming fermions and outgoing antifermions} \\ -1 & \text{for incoming antifermions and outgoing fermions} \end{cases} \quad (4.25)$$

and accounts for the sign difference of the charges of fermions and antifermions. In the high-energy limit we assume $M_W^2 \ll |r|$ for all kinematical invariants r that are not fixed to a certain mass value like $s_{34} = (p_3 + p_4)^2 = M_V^2$ after on-shell projection and keep only

logarithmic terms. If we apply this approximation to the non-factorizable corrections we find rather simple expressions for the quantities Δ_1 and Δ_2 :

$$\begin{aligned} \Delta_1(k_1, p_i; k_2, p_j) &= \frac{1}{2}(s_{ij}\bar{s} - \tilde{s}_{1j}\tilde{s}_{2i})D_0^{\text{he}}(-k_2 + p_j, k_1 + p_j, p_i + p_j, m_j, M_2, M_1, m_i) \\ &\quad + \ln \left(\frac{(k_2^2 - \overline{M}_2^2)M_1}{(k_1^2 - \overline{M}_1^2)M_2} \right) \ln \frac{\tilde{s}_{2i}}{\tilde{s}_{1j}} \\ &\quad + \left[2 + \ln \frac{s_{ij}}{\bar{s}} \right] \left[\ln \frac{\lambda M_2}{\overline{M}_2^2 - k_2^2} + \ln \frac{\lambda M_1}{\overline{M}_1^2 - k_1^2} \right], \end{aligned} \quad (4.26)$$

$$\Delta_2(p_k; k_l, p_j) = 2 \ln \frac{\lambda M_l}{\overline{M}_l^2 - k_l^2} \left[\ln \frac{\tilde{t}_{kl}}{t_{kj}} - 1 \right]. \quad (4.27)$$

The invariants are defined as $\tilde{s}_{ij} = (k_l + p_j)^2$, $\tilde{t}_{kl} = (p_k - k_l)^2$, $s_{ij} = (p_i + p_j)^2$, $t_{ij} = (p_i - p_j)^2$ and $\bar{s} = s_{12} = (p_1 + p_2)^2$ and have to be calculated using the appropriate on-shell-projected momenta. Note that the invariants \tilde{s}_{ij} , \tilde{t}_{kl} and \bar{s} differ from the corresponding invariants defined in (B.3) appearing in (A.16) and (A.17). It is crucial for the cancellation of the IR singularities that we use here the same definitions as in (4.2). In the high-energy limit we are interested in, the differences between the definitions disappear. In the D_0^{he} function, which is given in (B.30), also the on-shell-projected momenta enter. The original set of momenta enters the non-factorizable corrections only in the terms $k_l^2 - \overline{M}_l^2$, where $\overline{M}_l = \sqrt{M_l^2 - iM_l\Gamma_l}$ are the complex masses of the gauge bosons. We note that we could omit the first two lines of (4.26) in the logarithmic approximation since they do not contain large logarithms.

5 Treatment of soft and collinear photon emission

In this section we describe the treatment of soft and collinear photon emission. Soft and collinear singularities are regularized by an infinitesimal photon mass λ and small fermion masses, respectively. The masses of the external fermions are denoted by m_i ($p_i^2 = m_i^2 \rightarrow 0$).

5.1 Phase-space slicing

For the evaluation of the real corrections we use the phase-space slicing method, where the phase space is divided into singular and non-singular regions. The singular regions are integrated analytically thus allowing the explicit cancellation of the singularities against their counterparts in the virtual corrections. The finite remainder is evaluated by using Monte Carlo techniques.

For the actual implementation of this well-known procedure (see e.g. Ref. [25]) we closely follow the approach of Ref. [22]. We divide the five-particle phase space into soft, collinear, and finite regions by introducing the cut parameters δ_s and δ_c , respectively. The soft region contains photons with energies $E_\gamma < \delta_s \sqrt{\hat{s}}/2 = \Delta E$ in the CM frame of the incoming partons. The collinear region contains all photons with $E_\gamma > \Delta E$ but collinear

to any charged fermion, i.e. with $1 - \delta_c < \cos \theta_{\gamma f} < 1$, where $\theta_{\gamma f}$ is the angle between the charged fermion and the emitted photon in the partonic CM frame. The finite region contains all photons with $E_\gamma > \Delta E$ and $-1 < \cos \theta_{\gamma f} < 1 - \delta_c$ for all charged fermions.

In the soft and collinear regions, the squared matrix element $|\mathcal{M}^{\bar{q}_1 q_2 \rightarrow 4f\gamma}|^2$ factorizes into the leading-order squared matrix element $|\mathcal{M}_{\text{Born}}^{\bar{q}_1 q_2 \rightarrow 4f}|^2$ and a soft or collinear factor as long as δ_s and δ_c are sufficiently small. Also the five-particle phase space factorizes into a four-particle phase space, and a soft or collinear part. As a consequence the contribution of the real corrections can be written as

$$\int_{\Phi_{4f\gamma}} d\sigma_{\text{real}}^{\bar{q}_1 q_2 \rightarrow 4f\gamma} = \int_{\Phi_{4f\gamma}} d\sigma_{\text{finite}}^{\bar{q}_1 q_2 \rightarrow 4f\gamma} + \int_{\Phi_{4f}} d\sigma_{\text{soft}} + \int_{\Phi_{4f}} d\sigma_{\text{coll}}. \quad (5.1)$$

In the soft-photon region, we use the soft-photon approximation, i.e. the photon four-momentum k is omitted everywhere but in the IR-singular propagators. Since we neglect k also in the resonant gauge-boson propagators we have to assume $E_\gamma < \Delta E \ll \Gamma_V$, $V = W, Z$. In this region, $d\sigma^{\bar{q}_1 q_2 \rightarrow 4f\gamma}$ can be written as [26, 27]

$$d\sigma_{\text{soft}} = -d\sigma_{\text{Born}}^{\bar{q}_1 q_2 \rightarrow 4f} \frac{\alpha}{2\pi} \sum_{i=1}^6 \sum_{j=1}^6 Q_i Q_j \theta_d(i) \theta_d(j) I_{ij}, \quad (5.2)$$

where

$$I_{ij} = \frac{1}{2\pi} \int_{\substack{E_\gamma < \Delta E \\ |\mathbf{k}|^2 = E_\gamma^2 - \lambda^2}} \frac{d^3\mathbf{k}}{E_\gamma} \frac{p_i p_j}{(kp_i)(kp_j)}. \quad (5.3)$$

The explicit expression for the integrals I_{ij} can be found in Refs. [27, 28]. Since we only investigate high energies, we can assume that the energies E_i of the external fermions in the CM frame are large compared with their masses, $E_i \gg m_i$, and keep the fermion masses m_i only as regulators so that $d\sigma_{\text{soft}}$ can be written as

$$\begin{aligned} d\sigma_{\text{soft}} = & d\sigma_{\text{Born}}^{\bar{q}_1 q_2 \rightarrow 4f} \frac{\alpha}{2\pi} \sum_{i=1}^5 \sum_{j=i+1}^6 Q_i Q_j \theta_d(i) \theta_d(j) \left\{ 2 \ln \left(\frac{2\Delta E}{\lambda} \right) \right. \\ & \times \left[2 - \ln \left(\frac{s_{ij}^2}{m_i^2 m_j^2} \right) \right] - 2 \ln \left(\frac{4E_i E_j}{m_i m_j} \right) + \frac{1}{2} \ln^2 \left(\frac{4E_i^2}{m_i^2} \right) \\ & \left. + \frac{1}{2} \ln^2 \left(\frac{4E_j^2}{m_j^2} \right) + \frac{2\pi^2}{3} + 2 \text{Li}_2 \left(1 - \frac{4E_i E_j}{s_{ij}} \right) \right\}, \quad (5.4) \end{aligned}$$

where $s_{ij} = (p_i + p_j)^2$.

In the collinear region, we use the collinear limit, i.e. the components of the photon four-momentum k perpendicular to the momentum of the collinear fermion are omitted everywhere but in the singular propagators. The collinear cross section is divided into a part $d\sigma_{\text{coll}}^{\text{initial}}$ originating from initial-state radiation and a part $d\sigma_{\text{coll}}^{\text{final}}$ originating from final-state radiation,

$$d\sigma_{\text{coll}} = d\sigma_{\text{coll}}^{\text{initial}} + d\sigma_{\text{coll}}^{\text{final}}. \quad (5.5)$$

While the emission of photons from the final state does not change the kinematics of the subprocess, the initial-state radiation causes a loss of energy of the incoming partons. In the latter case assuming unpolarized incoming partons the cross section reads

$$d\sigma_{\text{coll}}^{\text{initial}} = \sum_{i=1,2} \frac{\alpha}{2\pi} Q_i^2 \int_0^{1-\delta_s} dz_i \left(\frac{1+z_i^2}{1-z_i} \ln \left(\frac{\hat{s}}{m_i^2} \frac{\delta_c}{2} \right) - \frac{2z_i}{1-z_i} \right) d\sigma_{\text{Born}}^{\bar{q}_1 q_2 \rightarrow 4f}(z_i p_i), \quad (5.6)$$

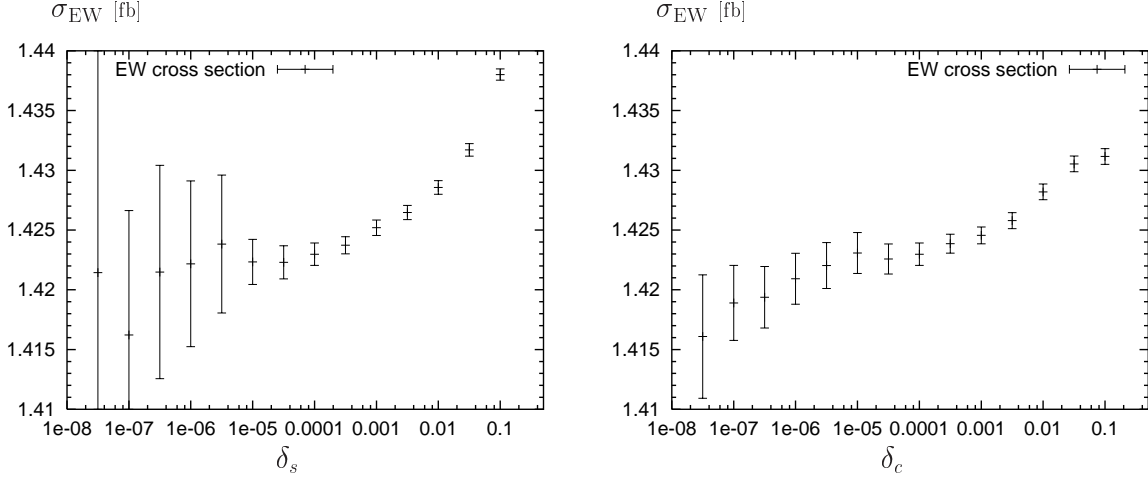


Figure 3: Dependence of the cross section for $\nu_e e^+ \mu^- \bar{\nu}_\mu$ production in the scenario (7.6) on the phase-space slicing cuts. Left: Dependence on δ_s for $\delta_c = 10^{-4}$. Right: Dependence on δ_c for $\delta_s = 10^{-4}$.

where z_i denotes the fraction of energy of the incoming parton i that is left after emission of the collinear photon, and \hat{s} is defined in (4.2). The differential cross section for final-state radiation reads

$$d\sigma_{\text{coll}}^{\text{final}} = \sum_{i=3}^6 \frac{\alpha}{2\pi} Q_i^2 \left(\left[\frac{3}{2} + 2 \ln \left(\frac{\Delta E}{E_i} \right) \right] \left[1 - \ln \left(\frac{4E_i^2 \delta_c}{m_i^2} \right) \right] + 3 - \frac{2\pi^2}{3} \right) d\sigma_{\text{Born}}^{\bar{q}_1 q_2 \rightarrow 4f}. \quad (5.7)$$

Note that this procedure implicitly assumes that photons within small cones collinear to charged final-state fermions will never be separated from those collinear fermions.

Subtracting the soft and collinear cross sections (5.4) and (5.5) from the cross section of the process $\bar{q}_1 q_2 \rightarrow 4f \gamma$ (5.1) yields the finite part $d\sigma_{\text{finite}}^{\bar{q}_1 q_2 \rightarrow 4f \gamma}$. The different contributions depend on the cut parameters δ_s and δ_c . The dependence on these technical cuts cancels in the sum when the cut parameters are chosen to be small enough so that the soft-photon and collinear approximations apply. The variation of the cross section for $\nu_e e^+ \mu^- \bar{\nu}_\mu$ production in the scenario (7.6) with the parameters δ_s and δ_c is shown in Fig. 3. While the numerical integration becomes unstable for very small cuts, and the soft and collinear approximations fail for too large cuts, the cross section is independent of the cuts within integration errors for $10^{-5} \lesssim \delta_s \lesssim 10^{-3}$ and $10^{-6} \lesssim \delta_c \lesssim 10^{-3}$. For the numerical analysis we have chosen $\delta_s = 10^{-4}$ and $\delta_c = 10^{-4}$.

5.2 Definition of finite virtual corrections

We fix the finite parts of $d\sigma_{\text{virt,sing}}^{\bar{q}_1 q_2 \rightarrow 4f}$ entering (2.12) by adopting the convention of Ref. [22],

$$d\sigma_{\text{virt,sing(DPA)}}^{\bar{q}_1 q_2 \rightarrow 4f} = d\sigma_{\text{Born(DPA)}}^{\bar{q}_1 q_2 \rightarrow 4f} \frac{\alpha}{2\pi} \sum_{i=1}^5 \sum_{j=i+1}^6 Q_i Q_j \theta_d(i) \theta_d(j)$$

$$\times \left[\mathcal{L}(s_{ij}, m_i^2) + \mathcal{L}(s_{ij}, m_j^2) + C_{ij} + C_{ji} \right] \quad (5.8)$$

with the invariants $s_{ij} = (p_i + p_j)^2$, the masses m_i of the external fermions, their relative charges Q_i , θ_d given by (4.25),

$$\mathcal{L}(s_{ij}, m_i^2) = \ln \frac{m_i^2}{s_{ij}} \ln \frac{\lambda^2}{s_{ij}} + \ln \frac{\lambda^2}{s_{ij}} - \frac{1}{2} \ln^2 \frac{m_i^2}{s_{ij}} + \frac{1}{2} \ln \frac{m_i^2}{s_{ij}}, \quad (5.9)$$

and the constant terms C_{ij} defined as

$$\begin{aligned} C_{ij} &= -\frac{\pi^2}{3} + 2, & \text{if } i \text{ and } j \text{ are incoming,} \\ C_{ij} &= \frac{\pi^2}{6} - 1, & \text{if } i \text{ is incoming and } j \text{ is outgoing,} \\ C_{ij} &= -\frac{\pi^2}{2} + \frac{3}{2}, & \text{if } i \text{ is outgoing and } j \text{ is incoming,} \\ C_{ij} &= -\frac{\pi^2}{3} + \frac{3}{2}, & \text{if } i \text{ and } j \text{ are outgoing.} \end{aligned} \quad (5.10)$$

Of course, in logarithmic approximation the constants C_{ij} could be omitted.

5.3 Absorption of mass singularities in parton distributions

After combining real and virtual corrections, the $\mathcal{O}(\alpha)$ -corrected partonic cross section still contains mass-singular terms of the form $\alpha \ln m_{q_k}$ involving the masses m_{q_k} of the incoming partons. These terms arise from collinear emission of photons in the initial state. In analogy to the $\overline{\text{MS}}$ factorization scheme for next-to-leading-order QCD corrections, we absorb these collinear singularities into the quark distributions. To this end, we replace the parton-distribution functions in (2.2) as

$$\begin{aligned} \Phi_{q,h}(x, Q^2) &\rightarrow \Phi_{q,h}(x, Q^2) - \frac{\alpha}{2\pi} Q_q^2 \int_x^1 \frac{dz}{z} \Phi_{q,h} \left(\frac{x}{z}, Q^2 \right) \\ &\times \left[\frac{1+z^2}{1-z} \left(\ln \frac{Q^2}{m_q^2} - 2 \ln(1-z) - 1 \right) \right]_+, \end{aligned} \quad (5.11)$$

where the usual $[\dots]_+$ prescription is defined by

$$\int_x^1 dz [f(z)]_+ g(z) = \int_x^1 dz f(z) g(z) - \int_0^1 dz f(z) g(1). \quad (5.12)$$

The replacement (5.11) amounts to a contribution

$$d\sigma_{\text{pdf}} = -\frac{\alpha}{2\pi} \sum_{i=1}^2 Q_i^2 \int_0^1 dz \left[\frac{1+z^2}{1-z} \left(\ln \frac{Q^2}{m_i^2} - 2 \ln(1-z) - 1 \right) \right]_+ d\sigma_{\text{Born}}^{\bar{q}_1 q_2 \rightarrow 4f}(z_i p_i) \quad (5.13)$$

that has to be added to the partonic cross section. When adding $d\sigma_{\text{pdf}}$ to $d\sigma_{\text{soft}}$, $d\sigma_{\text{coll}}$, and $d\sigma_{\text{virt,sing}}^{\bar{q}_1 q_2 \rightarrow 4f}$ all IR and collinear singularities, i.e. all $\ln(\lambda^2)$ and $\ln(m_i^2)$ terms, cancel.

The absorption of the collinear $\mathcal{O}(\alpha)$ singularities into the parton distributions requires also the inclusion of the corresponding corrections into the DGLAP evolution of these distributions and into their fit to experimental data. At present time there exist no published PDFs in which the photonic $\mathcal{O}(\alpha)$ corrections are consistently included. An approximative inclusion of the $\mathcal{O}(\alpha)$ corrections to the DGLAP evolution shows [29] that the impact of these corrections is below about 1%. Therefore, these effects are below our aimed accuracy of a few per cent and can be neglected.

6 Setup of the numerical analysis

We consider three classes of processes:

- (i) $pp \rightarrow l\nu_l l' \bar{l}'(+\gamma)$,
- (ii) $pp \rightarrow l \bar{l} l' \bar{l}'(+\gamma)$,
- (iii) $pp \rightarrow l \bar{\nu}_l \nu_l \bar{l}'(+\gamma)$,

where $l, l' = e$ or μ . In our notation, $l\nu_l$ indicates both $l^- \bar{\nu}_l$ and $l^+ \nu_l$. The first class is characterized by three isolated charged leptons plus missing energy in the final state. This channel includes WZ production as intermediate state. The second class is purely mediated by ZZ production, while the third class is related to $W^\pm W^\mp$ production. When there is a unique flavor in the final state, $l = l'$, the third process receives also a ZZ contribution.

All above-mentioned processes are described by (2.2). Since the two incoming hadrons are protons and we sum over final states with opposite charges, we find

$$\begin{aligned}
d\sigma^{\text{pp}}(P_1, P_2, p_f) = \int_0^1 dx_1 dx_2 \sum_{U=u,c} \sum_{D=d,s} & \left[\Phi_{\bar{D},p}(x_1, Q^2) \Phi_{U,p}(x_2, Q^2) d\hat{\sigma}^{\bar{D}U}(x_1 P_1, x_2 P_2, p_f) \right. \\
& + \Phi_{\bar{U},p}(x_1, Q^2) \Phi_{D,p}(x_2, Q^2) d\hat{\sigma}^{\bar{U}D}(x_1 P_1, x_2 P_2, p_f) \\
& + \Phi_{\bar{D},p}(x_2, Q^2) \Phi_{U,p}(x_1, Q^2) d\hat{\sigma}^{\bar{D}U}(x_2 P_2, x_1 P_1, p_f) \\
& \left. + \Phi_{\bar{U},p}(x_2, Q^2) \Phi_{D,p}(x_1, Q^2) d\hat{\sigma}^{\bar{U}D}(x_2 P_2, x_1 P_1, p_f) \right] \quad (6.1)
\end{aligned}$$

for WZ production and

$$\begin{aligned}
d\sigma^{\text{pp}}(P_1, P_2, p_f) = \int_0^1 dx_1 dx_2 \sum_{q=u,d,c,s} & \left[\Phi_{\bar{q},p}(x_1, Q^2) \Phi_{q,p}(x_2, Q^2) d\hat{\sigma}^{\bar{q}q}(x_1 P_1, x_2 P_2, p_f) \right. \\
& \left. + \Phi_{\bar{q},p}(x_2, Q^2) \Phi_{q,p}(x_1, Q^2) d\hat{\sigma}^{\bar{q}q}(x_2 P_2, x_1 P_1, p_f) \right] \quad (6.2)
\end{aligned}$$

for ZZ and WW production in leading order of QCD. Since the initial state is forward-backward symmetric for two incoming protons, this cross section is forward-backward symmetric.

For the free parameters we use the input values [30, 31]:

$$\begin{aligned}
G_\mu &= 1.16637 \times 10^{-5} \text{ GeV}^{-2}, & M_W &= 80.425 \text{ GeV}, & M_Z &= 91.1876 \text{ GeV}, \\
m_t &= 178.0 \text{ GeV}, & & & &
\end{aligned} \quad (6.3)$$

The weak mixing angle is fixed by $s_W^2 = 1 - M_W^2/M_Z^2$. Moreover, we adopted the so-called G_μ -scheme, which effectively includes higher-order contributions associated with the running of the electromagnetic coupling and the leading universal two-loop m_t -dependent corrections. To this end we parametrize the lowest-order matrix element in terms of the effective coupling $\alpha_{G_\mu} = \sqrt{2}G_\mu M_W^2 s_W^2/\pi = 7.543596\dots \times 10^{-3}$ and omit the explicit contributions proportional to $\Delta\alpha(M_W^2)$ and $\Delta\alpha(M_Z^2)$ in (4.19) and (4.23). In this setup our results are independent of the masses of the (internal) light quarks. Additional input parameters are the quark-mixing matrix elements whose values have been taken to be $V_{ud} = 0.974$ [32], $V_{cs} = V_{ud}$, $V_{us} = -V_{cd} = \sqrt{1 - |V_{ud}|^2} = 0.226548\dots$, $V_{tb} = 1$, and zero for all other matrix elements.

For the numerical results presented here, we have used the fixed-width scheme with Γ_Z and Γ_W from standard formulas

$$\Gamma_Z = \frac{\alpha M_Z}{24s_W^2 c_W^2} \left[21 - 40s_W^2 + \frac{160}{3}s_W^4 - 9\frac{m_b^2}{M_Z^2} + \frac{m_b^4}{M_Z^4} (24s_W^2 - 16s_W^4) + \frac{\alpha_s}{\pi} \left(15 - 28s_W^2 + \frac{88}{3}s_W^4 \right) \right] \quad (6.4)$$

and

$$\Gamma_W = \frac{\alpha M_W}{2s_W^2} \left[\frac{3}{2} + \frac{\alpha_s}{\pi} \right]. \quad (6.5)$$

Using $\alpha_s = 0.117$ for the strong coupling and $m_b = 4.9$ GeV we obtain

$$\Gamma_Z = 2.505044\dots \text{ GeV}, \quad \Gamma_W = 2.099360\dots \text{ GeV}. \quad (6.6)$$

As to parton distributions, we have used CTEQ6M [33] at the following factorization scales for the three classes of processes. We have chosen

$$Q^2 = \frac{1}{2} \left(M_W^2 + M_Z^2 + P_T^2(l\nu_l) + P_T^2(l'\bar{l}') \right) \quad (6.7)$$

for WZ production and

$$Q^2 = \frac{1}{2} \left(2M_Z^2 + P_T^2(l\bar{l}) + P_T^2(l'\bar{l}') \right) \quad (6.8)$$

for ZZ production, i.e. we use the transverse momentum P_T of the produced gauge bosons to fix Q^2 . For WW production, where the gauge bosons cannot be reconstructed, we take

$$Q^2 = \frac{1}{2} \left(2M_W^2 + P_T^2(l) + P_T^2(l') + P_T^2(\nu\nu') \right). \quad (6.9)$$

For final states that allow for two different sets of reconstructed gauge bosons, we choose the average of the corresponding scales from (6.7)–(6.9) if both reconstructed sets pass the cuts. This scale choice appears to be appropriate for the calculation of differential cross sections, in particular for vector-boson transverse-momentum distributions. It generalizes the scale of Refs. [3, 7] to final states with identical particles.

We have, moreover, implemented a general set of cuts, proper for LHC analyses, defined as follows:

- charged lepton transverse momentum $P_T(l) > 20$ GeV,
- missing transverse momentum $P_T^{\text{miss}} > 20$ GeV for final states with one neutrino and $P_T^{\text{miss}} > 25$ GeV for final states with two neutrinos,
- charged lepton pseudo-rapidity $|\eta_l| < 3$, where $\eta_l = -\ln(\tan(\theta_l/2))$, and θ_l is the polar angle of particle l with respect to the beam.

These cuts approximately simulate the detector acceptance. In addition to the above-mentioned cuts, we impose requirements on the separation of the charged lepton and the photon. We consider the following photon recombination procedure:

- Photons with a rapidity $|\eta_\gamma| > 3$ are treated as invisible.
- If the photon is central enough ($|\eta_\gamma| < 3$) and the rapidity–azimuthal-angle separation between charged lepton and photon $\Delta R_{l\gamma} = \sqrt{(\eta_l - \eta_\gamma)^2 + (\phi_l - \phi_\gamma)^2} < 0.1$, then the photon and lepton momentum four-vectors are combined into an effective lepton momentum.
- If the photon is central enough ($|\eta_\gamma| < 3$), the rapidity–azimuthal-angle separation $\Delta R_{l\gamma} > 0.1$, and the photon energy $E_\gamma < 2$ GeV, then the momenta of the photon and of the nearest charged lepton are recombined.

The effective lepton momentum must pass the acceptance cuts given above, and we use effective lepton momenta to define the above mentioned factorization scales.

For the processes considered, we have also implemented further cuts which are described in due time. In the following sections, we present results for the LHC at CM energy $\sqrt{s} = 14$ TeV and an integrated luminosity $L = 100$ fb⁻¹.

We have performed several consistency checks of our program. We showed that the cross sections do neither depend on the photon mass λ nor on the fermion masses m_f , which have been used as regulators. The independence of the phase-space-slicing parameters δ_s and δ_c has been checked as discussed in Sect. 5.1. Moreover, all results for WZ production have been verified by a second independent program at the level below 1%.

7 Phenomenological results

In the following, we discuss the phenomenological implications of the $\mathcal{O}(\alpha)$ EW corrections to vector-boson pair production at the LHC. We examine the impact of EW corrections on observables popularly employed to study anomalous gauge-boson couplings and vector-boson scattering. Systematic studies of the effect of anomalous couplings on the production of gauge-boson pairs have pointed out that in general deviations from the SM predictions should be particularly enhanced when gauge bosons are produced at high energies and large scattering angles in the di-boson rest frame [1]. The same kinematical region is also proper to search for the scattering of strongly interacting vector bosons. On the other hand, EW corrections are expected to be maximally pronounced in precisely these same regions. It is therefore interesting to discuss their effect in the aforesaid kinematical configuration.

In order to illustrate the behaviour and the size of the $\mathcal{O}(\alpha)$ contributions, we analyse different distributions according to the chosen final states. We work under the setup described in Sect. 6.

7.1 WZ production

First, we study the leptonic processes $pp \rightarrow l\nu_l l' \bar{l}'$ with $l, l' = e$ or μ . These final states can be mediated by WZ production and allow to test the trilinear WWZ coupling.

For this case we have chosen to investigate four distributions, two momentum distributions:

$P_T^{\max}(l)$: maximal transverse momentum of the three charged leptons,

P_T^{miss} : missing transverse momentum,

and two angular distributions:

$\Delta y(Zl) = y(Z) - y(l)$: difference of the rapidities of the reconstructed Z boson and the charged lepton from W-boson decay,

$y(l^-)$: rapidity of the negatively charged lepton coming from the reconstructed Z boson.

The rapidity is defined from the energy E and the longitudinal momentum P_L by $y = 0.5 \ln((E + P_L)/(E - P_L))$.

In addition to the standard cuts and the photon recombination recipe given in Sect. 6, we reconstruct the Z boson by imposing

$$|M(l'\bar{l}') - M_Z| < 20 \text{ GeV} \quad (7.1)$$

if $l \neq l'$. If identical particles are present in the final state, i.e. $l = l'$, we choose as reconstructed Z boson the lepton pair with invariant mass closer to M_Z . Since the neutrino produced in the leptonic W-boson decay cannot be directly detected, the longitudinal component of its momentum is not measurable. Therefore, there is not enough information to reconstruct the invariant mass of the W boson. Instead, the transverse mass defined as $M_T(l\nu_l) = \sqrt{E_T^2(l\nu_l) - P_T^2(l\nu_l)}$ is a physical quantity and can be restricted in order to isolate the doubly-resonant signal over the irreducible background. In the following, we require

$$M_T(l\nu_l) < M_W + 20 \text{ GeV}. \quad (7.2)$$

We note that under these kinematical cuts the exact result is well approximated by the DPA. The difference, which is about 15% without gauge-boson reconstruction, goes down to per-cent level (for a detailed discussion see Ref. [15]). Thus, we can safely adopt the DPA for calculating EW radiative corrections.

As an illustration of the role played by $\mathcal{O}(\alpha)$ corrections, we study the above-mentioned distributions in two different kinematical regions both characterized by large energies and scattering angles in the di-boson rest frame. As a first scenario, we restrict the transverse momentum of the reconstructed Z boson, $P_T(Z)$, by

$$P_T(Z) > 300 \text{ GeV}. \quad (7.3)$$

As a second scenario, we impose cuts on the invariant mass of the three charged leptons, $M_{\text{inv}}(l'l')$, and the difference $\Delta y(Zl) = y(Z) - y(l)$ between the rapidity of the reconstructed Z boson and of the charged lepton coming from the W-boson decay:

$$M_{\text{inv}}(l'l') > 500 \text{ GeV}, \quad |\Delta y(Zl)| < 3. \quad (7.4)$$

Under these cuts, all invariants $\hat{s}, \hat{t}, \hat{u}$ are large compared with the W-boson mass. In particular, $\sqrt{\hat{s}} \gtrsim 600 \text{ GeV}$ and $\sqrt{\hat{t}}, \sqrt{\hat{u}} \gtrsim 200 \text{ GeV}$ for most events and $\sqrt{\hat{s}} > 500 \text{ GeV}$ and $\sqrt{\hat{t}}, \sqrt{\hat{u}} > 100 \text{ GeV}$ for all. Thus, the conditions (2.13), under which the logarithmic high-energy approximation is valid, are fulfilled in these two kinematical regions.

We start discussing the scenario (7.3). In Fig. 4 we have plotted the four distributions for the complete process $pp \rightarrow e^- \bar{\nu}_e \mu^- \mu^+, \nu_e e^+ \mu^- \mu^+$, i.e. we sum over the two charge-conjugate final states. As a general feature the EW corrections are negative and lower the Born cross section by more than 10%. For the individual distributions we observe the following. EW corrections reduce the distribution in $P_{\text{T}}^{\text{max}}(l)$ by the order of 10% at low to modest $P_{\text{T}}^{\text{max}}(l)$ values. This effect grows with increasing $P_{\text{T}}^{\text{max}}(l)$ as shown by the long tail where the contribution of EW corrections can amount to more than 30%. This is of course the result of enhanced EW logarithms at large energies, which are enforced by the large $P_{\text{T}}^{\text{max}}(l)$. The missing-transverse-momentum distribution shows the same qualitative behaviour. At low values the correction amounts to about -12% , while at high $P_{\text{T}}^{\text{miss}}$ it increases up to -40% . As stated in the literature, the large P_{T} region is an ideal place to look for new physics. As an example, the $P_{\text{T}}(Z)$ distribution has been found to be much more sensitive to new-physics effects than the WZ invariant-mass distribution, which in principle should give a more direct access to the energy scale [6]. This feature is shared by $P_{\text{T}}^{\text{max}}(l)$ and $P_{\text{T}}^{\text{miss}}$ we just discussed.

As to angular distributions, EW corrections are maximal at low rapidity values in both cases, where once again effects due to new physics could be more enhanced. A low rapidity corresponds in fact to large scattering angles of the produced vector bosons in their rest frame. As shown in the lower left plot of Fig. 4, the distribution in the rapidity difference $\Delta y(Zl)$ exhibits a characteristic dip, relic of an approximate radiation zero at high energy [34]. Of course, new physics could have observable consequences on the shape of this variable [6]. The general tendency is to fill in the dip, but in certain models the approximate zero may even become more pronounced. It is thus important to consider the impact of radiative corrections to this relevant signal. In the last decade, the effect of NLO QCD corrections has been extensively analysed [6, 7]. It can completely spoil the significance of the dip, if one measures the inclusive $WZ + X$ production. By imposing a jet veto, the QCD corrections get drastically reduced to about 20% of the Born result, at the same time diminishing the dependence of the NLO cross section on the factorization scale. As shown in the third plot of Fig. 4, EW corrections can be of the same order as QCD effects but with opposite sign. So, they slightly increase the dip.

Of course, radiative corrections do not only depend on the considered distribution but also on the selected cuts. Figure 5 shows a second set of plots for the same set of distributions as above but in the scenario (7.4). The influence of the radiative corrections on the two momentum-like variables is analogous to the one observed in the previous case. The main difference between the two selected kinematical regions is in the shape of the $\Delta y(Zl)$ distribution. Here, the radiation-zero dip strongly increases. This is due to the

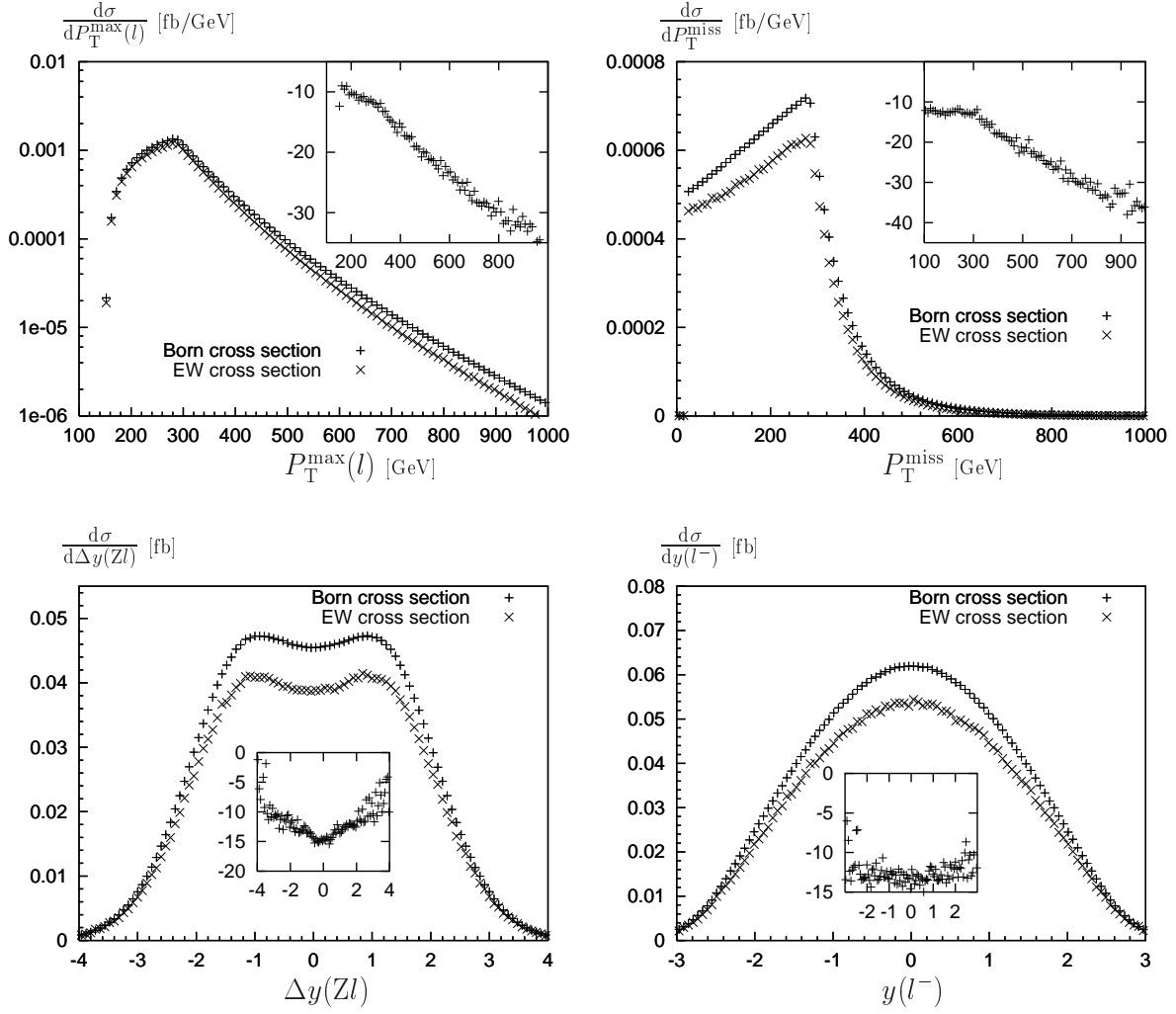


Figure 4: Distributions for WZ production: (a) Maximal transverse momentum of the charged leptons, (b) Missing transverse momentum. (c) Difference in rapidity between the reconstructed Z boson and the charged lepton coming from the W-boson decay. (d) Rapidity of the μ^- . The contributions of the final states $e^-\bar{\nu}_e\mu^-\mu^+$ and $\nu_e e^+\mu^-\mu^+$ are summed, and standard cuts as well as $P_T(Z) > 300$ GeV are applied. The inset plots show the $\mathcal{O}(\alpha)$ corrections relative to the Born results in per cent.

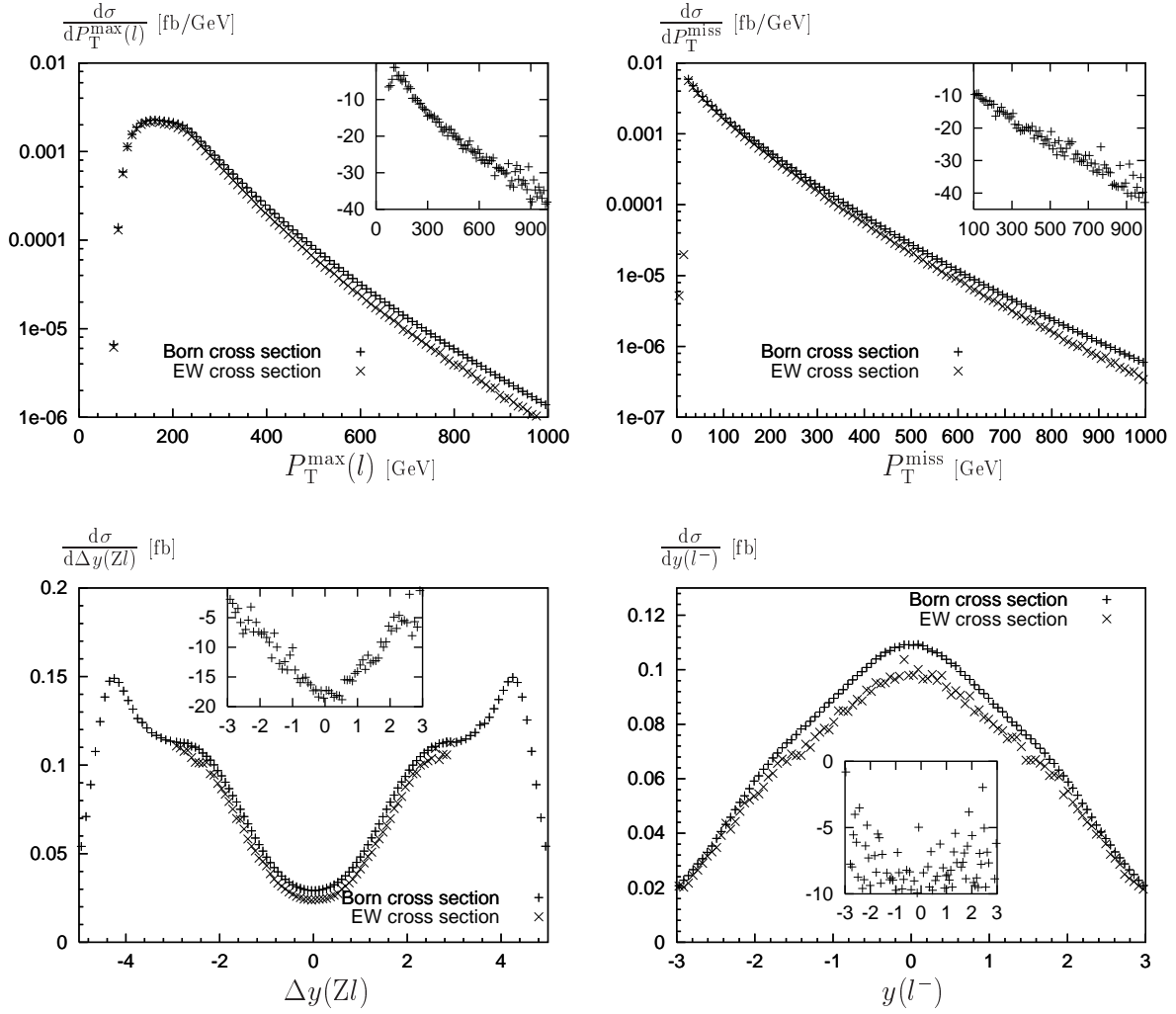


Figure 5: Distributions for WZ production: (a) Maximal transverse momentum of the charged leptons. (b) Missing transverse momentum. (c) Difference in rapidity between the reconstructed Z boson and the charged lepton coming from the W-boson decay. (d) Rapidity of the μ^- . The contributions of the final states $e^- \nu_e \mu^- \mu^+$ and $e^+ \bar{\nu}_e \mu^- \mu^+$ are summed, and standard cuts as well as $M_{\text{inv}}(l\bar{l}') > 500$ GeV and $|\Delta y(Zl)| < 3$ are applied. The last cut is omitted for the $\Delta y(Zl)$ distribution in lowest order. The inset plots show the $\mathcal{O}(\alpha)$ corrections relative to the Born results in per cent.

$pp \rightarrow l\nu_l l'\bar{l}'$						
$P_T^{\text{cut}}(Z)$ [GeV]	σ_{Born} [fb]	σ_{AEWS} [fb]	$\sigma_{\text{virt}}^{\text{finite}}$ [fb]	σ_{EW} [fb]	Δ [%]	$1/\sqrt{2L\sigma_{\text{Born}}}$ [%]
250	1.672	1.563	1.553	1.489	-10.9	5.5
300	0.876	0.794	0.789	0.761	-13.1	7.6
350	0.489	0.431	0.428	0.413	-15.5	10.1
400	0.287	0.246	0.244	0.236	-17.8	13.2
450	0.175	0.146	0.145	0.141	-19.7	16.9
500	0.111	0.090	0.089	0.087	-21.2	21.2

Table 1: Cross section for $pp \rightarrow l\nu_l l'\bar{l}'$ for various values of $P_T^{\text{cut}}(Z)$. Here we have summed over all eight final states with $l, l' = e$ or μ .

fact that the requirement $M_{\text{inv}}(ll'\bar{l}') > 500$ GeV forces the reconstructed Z boson and the charged lepton from the W-boson decay to be produced at large separation angle. This effect translates into a depletion of events in the central region of low rapidity difference. Radiative corrections are more pronounced in this suppressed region.

To measure the significance of the EW corrections, a naive but direct way is to compare their magnitude with the expected statistical error. In Table 1 we have listed the relative deviation Δ and the statistical accuracy, estimated by taking as a luminosity $L = 100 \text{ fb}^{-1}$ for two experiments, in the scenario (7.3) for some values of the cut on the transverse momentum of the reconstructed Z boson. To this purpose, we sum over all eight final states $e^- \bar{\nu}_e \mu^- \mu^+$, $\nu_e e^+ \mu^- \mu^+$, $\mu^- \bar{\nu}_\mu e^- e^+$, $\nu_\mu \mu^+ e^- e^+$, $\mu^- \bar{\nu}_\mu \mu^- \mu^+$, $\nu_\mu \mu^+ \mu^- \mu^+$, $e^- \bar{\nu}_e e^- e^+$, and $\nu_e e^+ e^- e^+$. In Table 2, we give the same entries but for the scenario (7.4) and for different values of the cut on the invariant mass of the three charged leptons. The integration errors in these and the following tables are at the level below 1%. The comparison of the expected statistical error with the EW corrections indicates that these are non-negligible and can be comparable with the experimental precision up to about $P_T^{\text{cut}}(Z) = 500$ GeV or $M_{\text{inv}}^{\text{cut}}(ll'\bar{l}') = 1$ TeV. In these regions the corrections range between -7 and -22%, being slightly more enhanced in the first scenario. Of course, their significance depends on the available luminosity. This kind of accuracy is needed only in a high-luminosity run.

Besides the lowest-order cross section σ_{Born} and the cross section σ_{EW} including the complete logarithmic EW corrections, we have also inserted two entries representing partial results in Tables 1 and 2 in order to give an idea of the individual contributions. The cross section including only the EW logarithms originating from above the EW scale, M_W , is denoted by σ_{AEWS} . This term neglects all IR- and mass-singular terms coming from the mass gap between the photon and the weak gauge bosons and is exactly the part computed in Ref. [15] for the same process. The column $\sigma_{\text{virt}}^{\text{finite}}$ contains instead the full finite virtual correction, i.e. the full logarithmic EW corrections with the IR- and mass-singular

pp $\rightarrow l\nu_l l'\bar{l}'$						
$M_{\text{inv}}^{\text{cut}}(ll'\bar{l}') [\text{GeV}]$	$\sigma_{\text{Born}} [\text{fb}]$	$\sigma_{\text{AEWS}} [\text{fb}]$	$\sigma_{\text{virt}}^{\text{finite}} [\text{fb}]$	$\sigma_{\text{EW}} [\text{fb}]$	$\Delta [\%]$	$1/\sqrt{2L\sigma_{\text{Born}}} [\%]$
500	1.729	1.689	1.692	1.601	-7.4	5.4
600	0.899	0.858	0.860	0.814	-9.5	7.5
700	0.508	0.474	0.476	0.452	-10.9	9.9
800	0.304	0.278	0.279	0.264	-13.3	12.8
900	0.190	0.170	0.171	0.161	-15.1	16.2
1000	0.123	0.108	0.109	0.102	-16.7	20.2

Table 2: Cross section for pp $\rightarrow l\nu_l l'\bar{l}'$ for $|\Delta y(Zl)| < 3$ and various values of $M_{\text{inv}}^{\text{cut}}(ll'\bar{l}')$. Here we have summed over all eight final states with $l, l' = e$ or μ .

contribution (5.8) subtracted. The difference between σ_{AEWS} and $\sigma_{\text{virt}}^{\text{finite}}$ is numerically small, despite of the fact that it contains logarithmic contributions. The dominant contribution to this difference is in fact proportional to $\alpha/(2\pi) \ln(s/M^2)[\ln(s/M^2) - 3]$ which is suppressed for energies between 500 GeV and 1 TeV owing to cancellations in the bracket.

7.2 ZZ production

In this section we extend our analysis to the processes pp $\rightarrow \bar{l}l'l'$ ($l, l' = e$ or μ). This channel is proper for studying the impact of trilinear neutral gauge-boson vertices, ZZZ and ZZ γ , on physical observables. While these couplings are absent in the SM Lagrangian, one-loop corrections induce small but not-vanishing values for them. Significantly larger couplings are predicted by non-standard models, where new physics appearing at energy scales much larger than those which can be directly probed at forthcoming experiments can be parametrized in terms of anomalous neutral self-interactions. At LEP2 and Tevatron, the ZZ γ vertex has been measured through Z γ production. LEP2 has been able to produce also ZZ pairs but with poor statistics. At the LHC several thousands of such ZZ pairs will be produced, allowing for more stringent bounds on ZZZ and ZZ γ vertices. The envisioned increase in statistics, and the possibility to observe significant deviations due to new physics interactions have gathered a renewed interest in the literature [35].

ZZZ and ZZ γ couplings affect the production of longitudinal or transverse Z bosons in a different way. Therefore, the helicity of the decay products coming from ZZ production constitutes a valuable information. Up to now, on one side the aforementioned studies have been performed in the *production* \times *decay* approach, neglecting all spin correlations and irreducible background contributions. On the other side, accurate calculations of QCD corrections have been carried out in Ref. [7]. In this section, we illustrate the results of a complete calculation of four-fermion production mediated by ZZ production

including logarithmic EW corrections. We focus, in particular, on the effect of the EW corrections on the distributions mostly discussed in the literature [36].

We consider the same kind of observables as in the previous section, with the only difference that we replace the distribution in the missing transverse momentum by the distribution in the maximal transverse momentum of the reconstructed Z bosons. To be precise we plot distributions in:

- $P_T^{\max}(l)$: maximal transverse momentum of the four charged leptons,
- $P_T(Z)$: maximal transverse momentum of the two reconstructed Z bosons,
- $\Delta y(ZZ)$: rapidity difference between the two reconstructed Z bosons,
- $y(\mu^-)$: rapidity of the μ^- .

The Z bosons are reconstructed by imposing (7.1), and for identical particles in the final state we choose the possibility where the reconstructed Z bosons are closer to their mass shell. We have checked that the accuracy of the DPA is at the level of a few per cent for this case.

We show results for the specific process $pp \rightarrow e^-e^+\mu^-\mu^+$ and only for the scenario characterized by the requirement

$$M_{\text{inv}}(\bar{l}l'\bar{l}') > 500 \text{ GeV}, \quad |\Delta y(ZZ)| < 3. \quad (7.5)$$

An analogous behaviour holds for the scenario with $P_T(Z) > 300 \text{ GeV}$ for both reconstructed Z bosons. We have verified that for both these scenarios the conditions (2.13) for the validity of the logarithmic high-energy approximation are fulfilled.

As one can see in Fig. 6, EW corrections modify the Born result in the same way as for WZ production, but the effect is typically a factor of 1.5 larger. We note that ZZ production at tree level does not present any true or approximate radiation zero. The dip in the distribution of the rapidity difference of the two reconstructed Z bosons results from the fact that the partonic process $q\bar{q} \rightarrow ZZ$, dominated by the transversely polarized Z bosons, is peaked forward and backward. Moreover, the dip is enhanced by the invariant mass cut in (7.5).

In Table 3 we compare the relative correction Δ to the Born cross section with the estimated experimental accuracy for some values of the cut on the partonic CM energy $M_{\text{inv}}(\bar{l}l'\bar{l}')$. To this purpose, we sum over all three final states $e^-e^+\mu^-\mu^+$, $e^-e^+e^-e^+$, and $\mu^-\mu^+\mu^-\mu^+$. The entries in Table 3 are defined as in the previous section. One can see that, compared to WZ production, $\mathcal{O}(\alpha)$ corrections manifest the same behaviour on the shown observables, but they are globally by a factor of ~ 1.5 larger. At modest ZZ invariant masses, the effect of the EW corrections can amount to two standard deviations, while it becomes comparable to the experimental precision with increasing CM energy. Of course, final states coming from ZZ production involving only charged leptons will not be copiously generated at the LHC. A detailed study of their properties would be possible only during a high-luminosity run. Although it yields higher statistics, we have not investigated ZZ production leading to $\bar{l}l\nu_l\bar{\nu}_l$ final states because there the reconstruction of the Z bosons is more problematic.

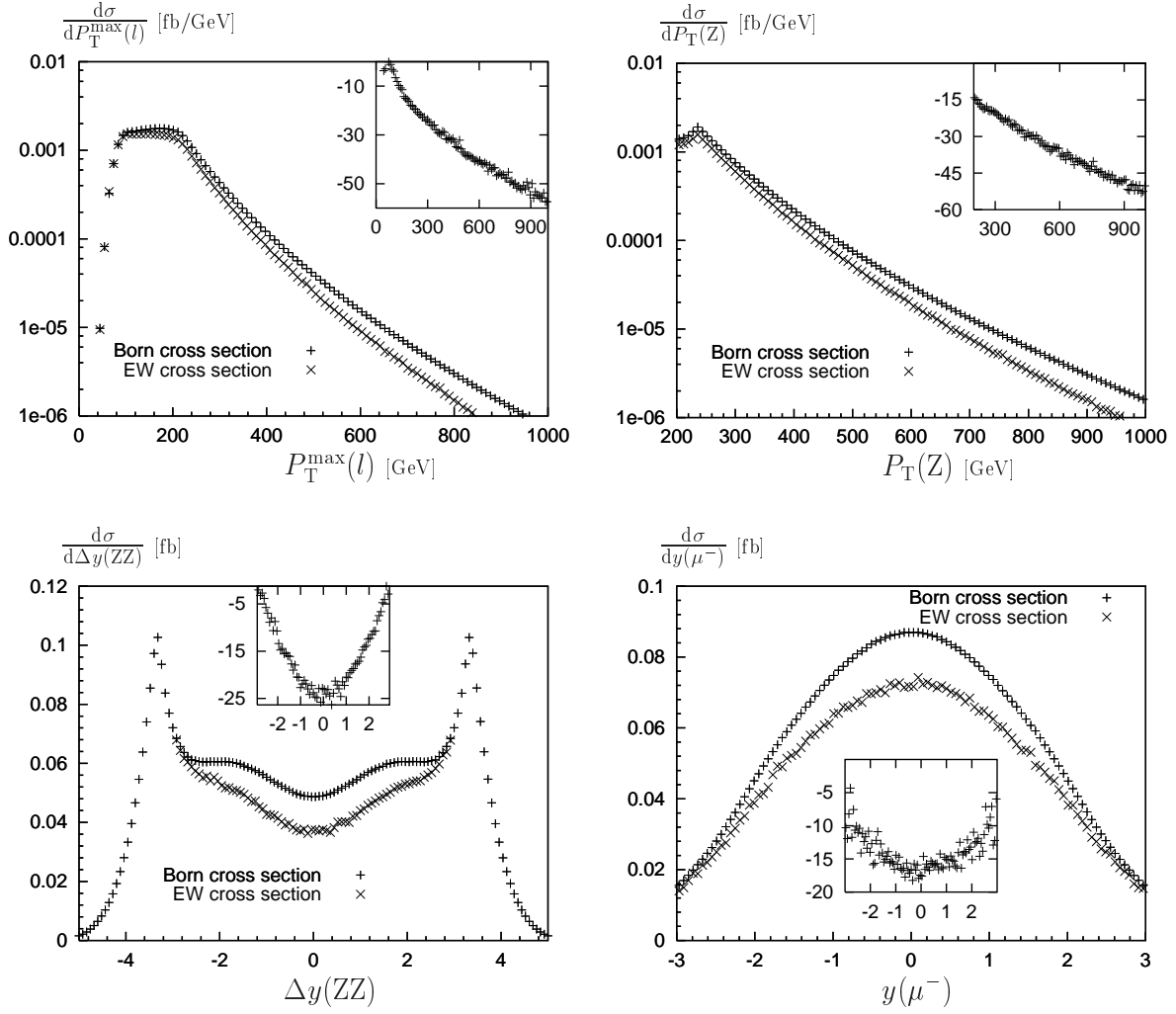


Figure 6: Distributions for ZZ production: (a) Maximal transverse momentum of the charged leptons. (b) Maximal transverse momentum of the reconstructed Z bosons. (c) Difference in rapidity between the two reconstructed Z bosons. (d) Rapidity of the μ^- . The final states is $e^-e^+\mu^-\mu^+$, and standard cuts as well as $M_{\text{inv}}(\ell\bar{\ell}\ell'\bar{\ell}') > 500$ GeV and $|\Delta y(ZZ)| < 3$ are applied. The last cut is omitted for the $\Delta y(ZZ)$ distribution in lowest order. The inset plots show the $\mathcal{O}(\alpha)$ corrections relative to the Born results in per cent.

pp $\rightarrow \bar{l}l'\bar{l}'$						
$M_{\text{inv}}^{\text{cut}}(\bar{l}l'\bar{l}')$ [GeV]	σ_{Born} [fb]	σ_{AEWS} [fb]	$\sigma_{\text{virt}}^{\text{finite}}$ [fb]	σ_{EW} [fb]	Δ [%]	$1/\sqrt{2L\sigma_{\text{Born}}}$ [%]
500	0.692	0.637	0.633	0.588	-15.0	8.5
600	0.356	0.314	0.312	0.291	-18.3	11.9
700	0.203	0.173	0.172	0.160	-21.0	15.7
800	0.123	0.102	0.101	0.094	-23.8	20.1
900	0.078	0.063	0.062	0.058	-26.1	25.3
1000	0.051	0.040	0.040	0.037	-28.1	31.2

Table 3: Cross section for pp $\rightarrow e^-e^+\mu^-\mu^+$, $e^-e^+e^-e^+$, and $\mu^-\mu^+\mu^-\mu^+$ for $|\Delta y(\text{ZZ})| < 3$ and various values of $M_{\text{inv}}^{\text{cut}}(\bar{l}l'\bar{l}')$

7.3 WW production

Finally, we discuss the processes pp $\rightarrow l\bar{\nu}_l\nu_{l'}\bar{l}'$ ($l, l' = e$ or μ). This channel contains information on the charged gauge-boson vertices WWZ and WW γ . While LEP2 could establish the non-abelian nature of the SM by measuring these couplings, high-precision measurements are still missing. At the LHC, the precision will be sensitively improved, if the large background from $t\bar{t}$ production can be properly controlled. The WW channel has in fact the largest cross section among all vector-boson pair-production processes. Despite the presence of two neutrinos, which do not allow a clean and unambiguous reconstruction of the two W bosons, the sensitivity to anomalous couplings is not seriously reduced. One can in fact consider the distribution in the missing transverse momentum [5].

For this channel, following the study of Ref. [7] on the sensitivity to new-physics effects, we choose to discuss distributions in the following variables:

$P_{\text{T}}^{\text{max}}(l)$: maximal transverse momentum of the two charged leptons,

$P_{\text{T}}^{\text{miss}}$: missing transverse momentum,

$\Delta y(\bar{l}l')$: rapidity difference between the charged leptons,

$y(l^-)$: rapidity of the negatively charged lepton.

Despite of the fact that we do not perform a reconstruction of the W bosons for these processes, the quality of the DPA is better than 10%. Since we apply the DPA only to the corrections and these are below 25%, at least where the cross section is appreciable, this introduces an error of only a few per cent. We consider the scenario

$$M_{\text{inv}}(\bar{l}l') > 500 \text{ GeV}, \quad |\Delta y(\bar{l}l')| < 3, \quad (7.6)$$

which fulfils the conditions (2.13) for the validity of the logarithmic high-energy approximation, as we have verified. Possible ZZ intermediate states are heavily suppressed by

the invariant-mass cut in (7.6). Therefore, we can safely neglect contributions of $\bar{l}l\nu_{l'}\bar{\nu}_{l'}$ final states with $l \neq l'$.

In Fig. 7 we show the distributions for the final state $\nu_e e^+ \mu^- \bar{\nu}_\mu$ with our standard cuts applied. As in the previous two cases, $\mathcal{O}(\alpha)$ corrections are enhanced at high energy and large scattering angles. This translates into larger radiative corrections in the tails of transverse momentum distributions and in the central region of rapidity distributions. Let us note that also in this case the partonic process at Born level does not vanish for any scattering angle, independently on the W-boson polarization. The dip appearing in the distribution of the rapidity difference between the two charged leptons is this time exclusively due to the chosen set of cuts. In absence of any kinematical cuts, the $pp \rightarrow W^+W^-$ process is dominated by the u-quark contribution, and the rapidity-difference $\Delta y(l\bar{l}')$ for the partonic process $\bar{u}u \rightarrow 4f$ is maximal and symmetric around zero. The requirement of having a large invariant mass of the two charged leptons, forces the two leptons to be produced at large separation angles. This fact depletes the number of events in the central region of $\Delta y(l\bar{l}')$ and leaves events with larger rapidity difference. This gives rise to the shape of Fig. 7.

The general behaviour of EW corrections does not present novelties compared to the previous cases. The interesting feature of WW processes is the remarkable statistics of purely leptonic final states. As shown in Table 4, where we sum over the four final states $e^- \bar{\nu}_e \nu_\mu \mu^+$, $\mu^- \bar{\nu}_\mu \nu_e e^+$, $\mu^- \bar{\nu}_\mu \nu_\mu \mu^+$, and $e^- \bar{\nu}_e \nu_e e^+$, the estimated experimental precision is around a few per cent at CM energies below 700 GeV. On the other hand, the deviation from the Born result given by the $\mathcal{O}(\alpha)$ contributions ranges between -14 and -18% in the same energy domain. At larger invariant masses, the overall cross section decreases but radiative corrections are still of order 2–3 standard deviations. Thus, a reliable analysis of these final states requires the inclusion of EW corrections. Note also that, in contrast to previous processes, $\mathcal{O}(\alpha)$ corrections can be relevant even in the low-luminosity run ($L = 30 \text{ fb}^{-1}$). They are about twice the standard deviation for $M_{\text{inv}}^{\text{cut}}(l\bar{l}') \leq 700 \text{ GeV}$, and become comparable with the experimental accuracy above that threshold.

8 Conclusion

At the LHC, gauge-boson production processes will be used for precise measurements of the triple gauge-boson couplings. The relevant processes to investigate are WZ, ZZ, and WW production, and the physically interesting region is the one of high di-boson invariant mass.

We have examined these processes by means of a complete four-fermion calculation, i.e. by taking into account the decays of the gauge bosons, in the purely leptonic channels. The primary aim of our analysis was to investigate the influence of electroweak radiative corrections on the di-boson production processes at the LHC. The one-loop logarithmic corrections to the full four-fermion processes have been calculated in double-pole approximation. This includes corrections to the gauge-boson-pair-production processes, corrections to the gauge-boson decays, as well as non-factorizable corrections. In this study, we have included the full electromagnetic radiative corrections in the logarithmic approximation, which involve also the emission of real photons and therefore depend on

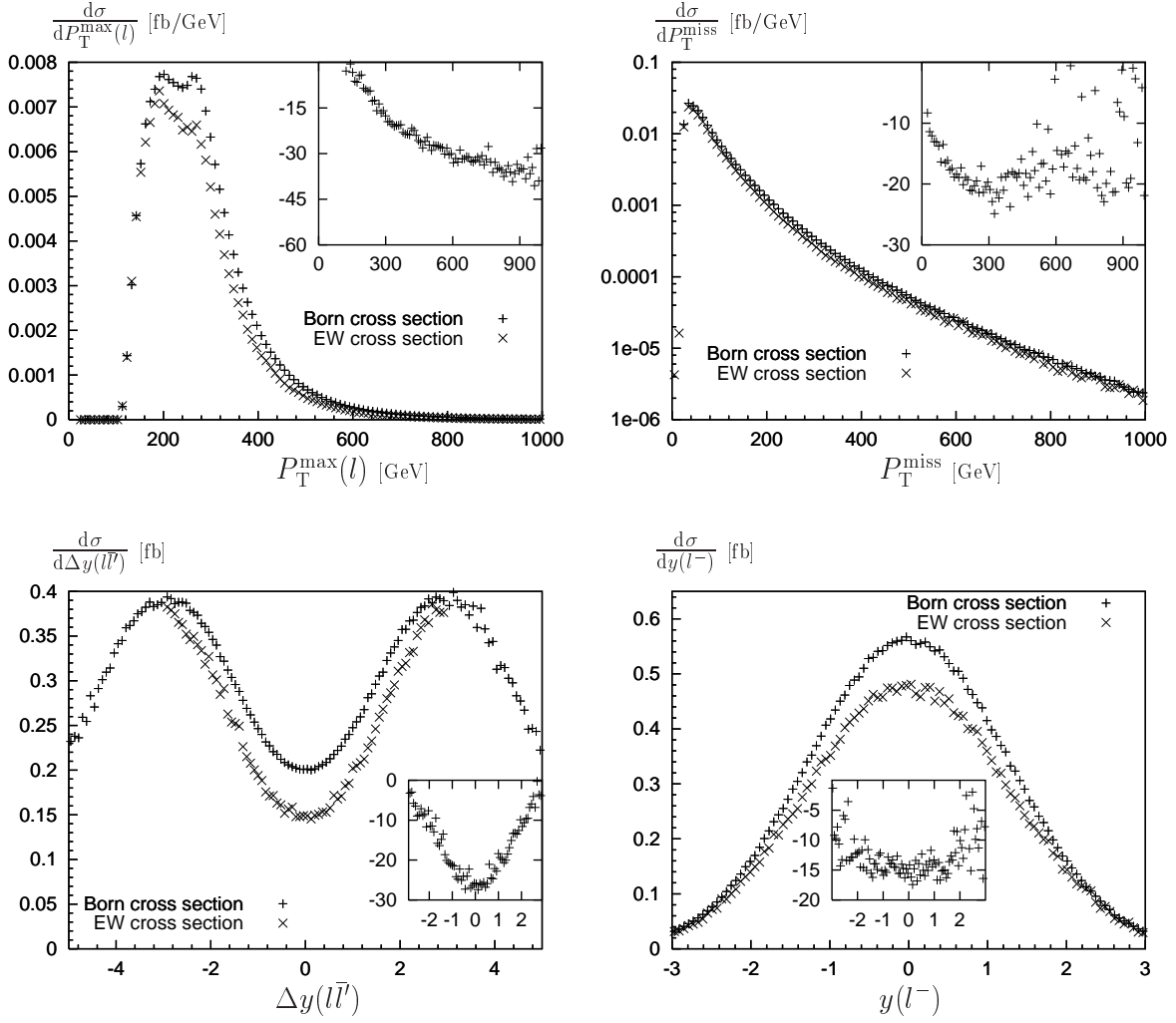


Figure 7: Distributions for WW production: (a) Maximal transverse momentum of the charged leptons. (b) Missing transverse momentum. (c) Difference in rapidity between the two charged leptons. (d) Rapidity of the negatively charged lepton. The final state is $\nu_e e^+ \mu^- \bar{\nu}_\mu$ with standard cuts as well as $M_{\text{inv}}(l\bar{l}') > 500$ GeV and $|\Delta y(l\bar{l}')| < 3$ applied. The last cut is omitted to the $\Delta y(l\bar{l}')$ distribution in lowest order. The inset plots show the $\mathcal{O}(\alpha)$ corrections relative to the Born results in per cent.

pp $\rightarrow l\bar{\nu}_l\nu_l\bar{l}'$						
$M_{\text{inv}}^{\text{cut}}(l\bar{l}') [\text{GeV}]$	$\sigma_{\text{Born}} [\text{fb}]$	$\sigma_{\text{AEWS}} [\text{fb}]$	$\sigma_{\text{virt}}^{\text{finite}} [\text{fb}]$	$\sigma_{\text{EW}} [\text{fb}]$	$\Delta [\%]$	$1/\sqrt{2L\sigma_{\text{Born}}} [\%]$
500	7.235	6.561	6.682	6.235	-13.8	2.6
600	3.723	3.280	3.350	3.131	-15.9	3.7
700	2.059	1.765	1.808	1.688	-18.1	4.9
800	1.201	1.003	1.031	0.959	-20.2	6.5
900	0.731	0.596	0.613	0.570	-22.0	8.3
1000	0.460	0.366	0.378	0.352	-23.4	10.4

Table 4: Cross section for pp $\rightarrow e^-\bar{\nu}_e\nu_e\mu^+, \mu^-\bar{\nu}_\mu\nu_\mu e^+, \mu^-\bar{\nu}_\mu\nu_\mu\mu^+, e^-\bar{\nu}_e\nu_e e^+$ for $|\Delta y(l\bar{l}')| < 3$ and various values of $M_{\text{inv}}^{\text{cut}}(l\bar{l}')$

the detector resolution. We have verified that the double-pole approximation and the high-energy approximation are applicable for the considered phase-space regions of large transverse momentum or large invariant mass of the gauge-boson pair. Thus, our approach is reliable in this region. The corrections have been implemented in a Monte Carlo program, so that arbitrary cuts and distributions can be studied.

In order to illustrate the behaviour and the size of $\mathcal{O}(\alpha)$ contributions, we have presented different cross sections and distributions. For WZ-, ZZ-, and WW-production processes, electroweak corrections turn out to be sizeable in the high-energy region of the hard process, in particular for large transverse momentum and small rapidity separation of the reconstructed vector bosons, which is the kinematical range of maximal sensitivity to new-physics phenomena. Electroweak radiative corrections lower the Born results for WZ, ZZ, and WW production by 7–22%, 15–28%, and 14–24%, in the region of experimental sensitivity. Their size depends sensibly not only on the CM energy but also on the applied cuts and varies according to the selected observables and kinematical regions. Despite of the strong decrease of the cross section with increasing di-boson invariant mass, radiative effects are appreciable if compared with the expected experimental precision. This depends of course on the available luminosity. For WZ and ZZ production, these effects are only relevant for a high-luminosity run of the LHC. Owing to their larger overall cross section, WW-production processes can instead show a sensitivity to radiative effects even at a low-luminosity run.

Acknowledgements

We thank M. Roth for his invaluable help concerning the Monte Carlo generator and S. Pozzorini for his contributions in the evaluation of the logarithmic corrections. This work was supported in part by the Swiss Bundesamt für Bildung und Wissenschaft, by the European Union under contract HPRN-CT-2000-00149, and by the Italian Ministero

Appendix

A Non-factorizable photonic corrections

In this appendix we generalize the results of Refs. [22, 37] for the virtual non-factorizable corrections to a general class of processes.

A.1 Conventions and notations

We start by discussing non-factorizable corrections to the generic process

$$g_1(p_1) + g_2(p_2) \rightarrow \sum_{l=1}^N R_l(k_l) + \sum_{j=1}^{n_0} f_{0j}(q_{0j}) \rightarrow \sum_{l=1}^N \sum_{i=1}^{n_l} f_{li}(q_{li}) + \sum_{j=1}^{n_0} f_{0j}(q_{0j}). \quad (\text{A.1})$$

Two incoming particles g_1 and g_2 with momenta p_1 and p_2 , masses m'_1 and m'_2 , and charges Q'_1 and Q'_2 scatter into N resonances R_l with momenta k_l , masses M_l , decay widths Γ_l , and charges Q_l and n_0 stable particles f_{0j} with momenta q_{0j} , masses m_{0j} , and charges Q_{0j} . Each resonance R_l then decays into n_l stable massless particles with momenta q_{li} , masses m_{li} , and charges Q_{li} . Whereas the charges Q'_k are incoming, all charges Q_l and Q_{li} are assumed to be outgoing. The masses of the external particles, which are typically light fermions, are neglected, except where this would lead to mass singularities. The complex masses squared of the resonances are denoted by

$$\overline{M}_l^2 = M_l^2 - iM_l\Gamma_l, \quad (\text{A.2})$$

and we introduce the off-shellness variables

$$K_l = k_l^2 - M_l^2. \quad (\text{A.3})$$

We want to give the non-factorizable corrections to the process (A.1) in leading-pole approximation (LPA). The LPA takes into account only the leading terms in an expansion around the poles originating from the propagators of the resonances. For two resonances, the LPA is just the double-pole approximation used in the main part of this paper. In LPA, the lowest-order matrix element for process (A.1) factorizes into the matrix element for the production of the N on-shell resonances, $\mathcal{M}_{\text{Born}}^{g_1 g_2 \rightarrow R_1 \dots R_N f_{01} \dots f_{0n_0}}(p_1, p_2, k_l, q_{0j})$, the propagators³ of these resonances, and the matrix elements for the decays of these on-shell resonances, $\mathcal{M}_{\text{Born}}^{R_l \rightarrow f_{l1} \dots f_{ln_l}}(k_l, q_{li})$:

$$\mathcal{M}_{\text{Born}} = \sum_{\text{pol}} \mathcal{M}_{\text{Born}}^{g_1 g_2 \rightarrow R_1 \dots R_N f_{01} \dots f_{0n_0}} \prod_{l=1}^N \frac{\mathcal{M}_{\text{Born}}^{R_l \rightarrow f_{l1} \dots f_{ln_l}}}{K_l}. \quad (\text{A.4})$$

The sum runs over the physical polarizations of the resonances.

³For gauge bosons only the physical transverse parts enter.

A.2 Generic form of the correction factor

The non-factorizable EW corrections result exclusively from the exchange of photons that connect the production and decay subprocesses or two decay subprocesses [37, 38, 39]. Only photons with energies of the order of the decay widths or smaller are relevant so that an extended soft-photon approximation, which takes into account the dependence of the resonant propagators on the photon momenta, can be used. Consequently, the non-factorizable corrections $d\sigma_{\text{nf}}$ to the fully differential lowest-order cross section $d\sigma_{\text{Born}}$ resulting from the matrix element (A.4) take the form of a correction factor to the lowest-order cross section:

$$d\sigma_{\text{nf,LPA}}^{\text{virt}} = \delta_{\text{nf,LPA}}^{\text{virt}} d\sigma_{\text{Born,LPA}}. \quad (\text{A.5})$$

The non-factorizable corrections get contributions from virtual photons exchanged between a resonance and its decay products (mf), between the production process and a resonance (im), between the production process and the decay products of a resonance (if), between two resonances (mm'), between a resonance and the decay products of another resonance (mf'), between decay products of different resonances (ff'), and virtual photons attached to one resonance (mm). Examples can be found in Figures 1 and 2 of Ref. [37] or in Figure 2 of Ref. [22].

Upon splitting the contributions that result from photons coupled to the charged resonances according to $Q_l = \sum_i Q_{li}$ into contributions associated with definite final-state fermions and using $Q'_1 + Q'_2 = \sum_{l=0}^N \sum_{i=1}^{n_l} Q_{li}$ to rewrite the terms originating from the (mf) and (mm) contributions, the complete correction factor to the lowest-order cross section can be written as

$$\begin{aligned} \delta_{\text{nf,LPA}}^{\text{virt}} = & - \sum_{l=1}^{N-1} \sum_{m=l+1}^N \sum_{i=1}^{n_l} \sum_{j=1}^{n_m} Q_{li} Q_{mj} \frac{\alpha}{\pi} \text{Re}\{\Delta_1(k_l, q_{li}; k_m, q_{mj})\} \\ & - \sum_{k=1}^2 \sum_{l=1}^N \sum_{i=1}^{n_l} Q'_k Q_{li} \frac{\alpha}{\pi} \text{Re}\{\Delta_2(p_k; k_l, q_{li})\} \\ & + \sum_{j=1}^{n_0} \sum_{l=1}^N \sum_{i=1}^{n_l} Q_{0j} Q_{li} \frac{\alpha}{\pi} \text{Re}\{\Delta_2(-q_{0j}; k_l, q_{li})\}. \end{aligned} \quad (\text{A.6})$$

The quantity Δ_1 gets contributions from $\Delta_{\text{mm}'}^{\text{virt}}$, $\Delta_{\text{mf}'}^{\text{virt}}$, $\Delta_{\text{ff}'}^{\text{virt}}$, $\Delta_{\text{mf}}^{\text{virt}}$, and $\Delta_{\text{mm}}^{\text{virt}}$,

$$\begin{aligned} \Delta_1(k_l, q_{li}; k_m, q_{mj}) = & (\Delta_{\text{mm}'}^{\text{virt}} + \Delta_{\text{mf}'}^{\text{virt}} + \Delta_{\text{ff}'}^{\text{virt}})(k_l, q_{li}; k_m, q_{mj}) \\ & - (\Delta_{\text{mf}}^{\text{virt}} + \Delta_{\text{mm}}^{\text{virt}})(k_l, q_{li}) - (\Delta_{\text{mf}}^{\text{virt}} + \Delta_{\text{mm}}^{\text{virt}})(k_m, q_{mj}), \end{aligned} \quad (\text{A.7})$$

and Δ_2 gets contributions from $\Delta_{\text{im}}^{\text{virt}}$, $\Delta_{\text{if}}^{\text{virt}}$, $\Delta_{\text{mf}}^{\text{virt}}$, and $\Delta_{\text{mm}}^{\text{virt}}$,

$$\Delta_2(p_k; k_l, q_{li}) = (\Delta_{\text{im}}^{\text{virt}} + \Delta_{\text{if}}^{\text{virt}})(p_k; k_l, q_{li}) + (\Delta_{\text{mf}}^{\text{virt}} + \Delta_{\text{mm}}^{\text{virt}})(k_l, q_{li}). \quad (\text{A.8})$$

The contributions of the different types of diagrams are given by

$$\begin{aligned} \Delta_{\text{ff}'}^{\text{virt}} & \sim -2(q_{li} q_{mj}) K_l K_m E_0(-q_{mj}, -k_m, k_l, q_{li}, \lambda, m_{mj}, \overline{M}_m, \overline{M}_l, m_{li}), \\ \Delta_{\text{mf}'}^{\text{virt}} & \sim -2(k_l q_{mj}) K_m D_0(-q_{mj}, -k_m, k_l, 0, m_{mj}, \overline{M}_m, \overline{M}_l) \\ & \quad - 2(k_m q_{li}) K_l D_0(-q_{li}, -k_l, k_m, 0, m_{li}, \overline{M}_l, \overline{M}_m), \end{aligned}$$

$$\begin{aligned}
\Delta_{\text{if}}^{\text{virt}} &\sim -2(p_k q_l) K_l D_0(p_k, k_l, q_l, \lambda, m'_k, \overline{M}_l, m_{li}), \\
\Delta_{\text{mm}'}^{\text{virt}} &\sim -2(k_l k_m) \left\{ C_0(k_l, -k_m, 0, \overline{M}_l, \overline{M}_m) - \left[C_0(k_l, -k_m, \lambda, M_l, M_m) \right]_{k_{l,m}^2 = M_{l,m}^2} \right\}, \\
\Delta_{\text{im}}^{\text{virt}} &\sim -2(p_k k_l) \left\{ C_0(p_k, k_l, 0, m'_k, \overline{M}_l) - \left[C_0(p_k, k_l, \lambda, m'_k, M_l) \right]_{k_l^2 = M_l^2} \right\}, \\
\Delta_{\text{mf}}^{\text{virt}} &\sim -2(k_l q_l) \left\{ C_0(k_l, q_l, 0, \overline{M}_l, m_{li}) - \left[C_0(k_l, q_l, \lambda, M_l, m_{li}) \right]_{k_l^2 = M_l^2} \right\}, \\
\Delta_{\text{mm}}^{\text{virt}} &\sim -2M_l^2 \left\{ \frac{B_0(k_l^2, 0, \overline{M}_l) - B_0(\overline{M}_l^2, 0, \overline{M}_l)}{k_l^2 - \overline{M}_l^2} - B'_0(M_l^2, \lambda, M_l) \right\}. \tag{A.9}
\end{aligned}$$

Note that these definitions deviate partially in sign and form from those used in Refs. [22, 37]. The symbol “ \sim ” in (A.9) indicates that the limits $k_l^2 \rightarrow M_l^2$ and $\Gamma_l \rightarrow 0$ are implicitly understood whenever possible. The definition of the scalar integrals B_0 , C_0 , D_0 , E_0 and of their arguments can be found in Refs. [27, 37]. The explicit expressions of these functions have been given in Refs. [22, 37] for equal masses of the resonances. The generalized expressions for arbitrary masses are listed in Appendix B.

A.3 Simplifications of the generic correction factor

Using the explicit expression for the loop integrals given in Appendix B.1, the terms in the correction factor can be simplified. The results given in the following are only valid for $(k_l - q_i)^2 = 0$, which holds if the resonances decay into two massless particles.

The sum $\Delta_{\text{mf}'}^{\text{virt}} + \Delta_{\text{ff}'}^{\text{virt}}$ can be simplified by inserting the decompositions of the 5-point function (B.22). In LPA this leads to

$$\begin{aligned}
(\Delta_{\text{mf}'}^{\text{virt}} + \Delta_{\text{ff}'}^{\text{virt}})(k_m, q_j; k_l, q_i) &\sim \frac{K_l K_m s_{ij} \det(Y_0)}{\det(Y)} D_0(0) \\
&+ \frac{K_l \det(Y_3)}{\det(Y)} \left\{ [K_l \tilde{s}_{mi} + K_m M_l^2] D_0(1) + K_m s_{ij} D_0(3) \right\} \\
&+ \frac{K_m \det(Y_2)}{\det(Y)} \left\{ [K_m \tilde{s}_{lj} + K_l M_m^2] D_0(4) + K_l s_{ij} D_0(2) \right\}, \tag{A.10}
\end{aligned}$$

where s_{ij} and \tilde{s}_{lj} are defined in (B.3) and $D_0(l)$ in (B.17). Note that $\Delta_{\text{mf}'}^{\text{virt}}$ is exactly cancelled by the contributions of the last two terms in (B.22). Inserting the expressions for the scalar integrals into the different contributions, we find using the first relation in (B.21)

$$\begin{aligned}
&(\Delta_{\text{mf}'}^{\text{virt}} + \Delta_{\text{ff}'}^{\text{virt}})(k_m, q_j; k_l, q_i) - \Delta_{\text{mf}}^{\text{virt}}(k_m, q_j) - \Delta_{\text{mf}}^{\text{virt}}(k_l, q_i) \\
&\sim \frac{K_l K_m s_{ij} \det(Y_0)}{\det(Y)} D_0(0) + \frac{K_l \det(Y_3)}{\det(Y)} F(k_m, q_j; k_l, q_i) \\
&+ \frac{K_m \det(Y_2)}{\det(Y)} F(k_l, q_i; k_m, q_j) + \ln\left(\frac{\lambda^2}{M_l M_m}\right) \ln\left(-\frac{s_{ij}}{M_l M_m} - i\epsilon\right) \tag{A.11}
\end{aligned}$$

with $D_0(0)$ given in (B.13) and

$$\begin{aligned}
F(k_m, q_j; k_l, q_i) &= [K_l \tilde{s}_{mi} + K_m M_l^2] D_0(1) + K_m s_{ij} D_0(3) \\
&+ \ln\left(\frac{\lambda^2}{M_l M_m}\right) \ln\left(-\frac{s_{ij}}{M_l M_m} - i\epsilon\right) \\
&- M_l^2 \left\{ C_0(k_l, q_i, 0, \overline{M}_l, m_i) - [C_0(k_l, q_i, \lambda, M_l, m_i)]_{k_l^2=M_l^2} \right\} \\
&- M_m^2 \left\{ C_0(k_m, q_j, 0, \overline{M}_m, m_j) - [C_0(k_m, q_j, \lambda, M_m, m_j)]_{k_m^2=M_m^2} \right\} \\
&= \sum_{\tau=\pm 1} \left[\mathcal{L}i_2\left(\frac{K_l M_m}{K_m M_l}, r_{lm}^\tau\right) - \mathcal{L}i_2\left(-\frac{M_l M_m}{\tilde{s}_{mi}} + i\epsilon, r_{lm}^\tau\right) \right] \\
&- 2 \mathcal{L}i_2\left(\frac{K_l M_m}{K_m M_l}, -\frac{\tilde{s}_{mi}}{M_l M_m} - i\epsilon\right) - \text{Li}_2\left(1 - \frac{\tilde{s}_{mi}}{s_{ij}}\right) - \ln^2\left(-\frac{\tilde{s}_{mi}}{M_l M_m} - i\epsilon\right) \\
&+ \ln\left(-\frac{s_{ij}}{M_l M_m} - i\epsilon\right) \left[\ln\left(-\frac{K_m}{M_l M_m}\right) + \ln\left(-\frac{K_m}{M_m^2}\right) \right]. \tag{A.12}
\end{aligned}$$

The dilogarithms Li_2 , $\mathcal{L}i_2$ are defined in (B.5) and (B.6). The quantity Δ_1 is then obtained from (A.11) and

$$\begin{aligned}
\Delta_{\text{mm}}^{\text{virt}}(k_l, q_i) &= -2 \ln\left(\frac{\lambda M_l}{-K_l}\right) - 2, \\
\Delta_{\text{mm}'}^{\text{virt}}(k_m, q_j; k_l, q_i) &= -\bar{s}_{lm} \left\{ C_0(k_l, -k_m, 0, \overline{M}_l, \overline{M}_m) - [C_0(k_l, -k_m, \lambda, M_l, M_m)]_{k_l^2=M_l^2} \right\} \tag{A.13}
\end{aligned}$$

as

$$\begin{aligned}
\Delta_1(k_m, q_j; k_l, q_i) &\sim \frac{K_l K_m s_{ij} \det(Y_0)}{\det(Y)} D_0(0) + \frac{K_l \det(Y_3)}{\det(Y)} F(k_m, q_j; k_l, q_i) \\
&+ \frac{K_m \det(Y_2)}{\det(Y)} F(k_l, q_i; k_m, q_j) + \ln\left(\frac{\lambda^2}{M_l M_m}\right) \ln\left(-\frac{s_{ij}}{M_l M_m} - i\epsilon\right) \\
&- \bar{s}_{lm} \left\{ C_0(k_l, -k_m, 0, \overline{M}_l, \overline{M}_m) - [C_0(k_l, -k_m, \lambda, M_l, M_m)]_{k_l^2=M_l^2} \right\} \\
&+ 2 \ln\left(\frac{\lambda M_l}{-K_l}\right) + 2 \ln\left(\frac{\lambda M_m}{-K_m}\right) + 4. \tag{A.14}
\end{aligned}$$

When inserting the explicit expressions for the integrals, the quantity Δ_2 simplifies to

$$\begin{aligned}
\Delta_2(p_k; k_l, q_i) &= (\Delta_{\text{im}}^{\text{virt}} + \Delta_{\text{if}}^{\text{virt}})(p_k; k_l, q_i) + (\Delta_{\text{mf}}^{\text{virt}} + \Delta_{\text{mm}}^{\text{virt}})(k_l, q_i) \\
&= 2 \ln\left(\frac{\lambda M_l}{-K_l}\right) \left[\ln\left(\frac{\tilde{t}_{kl}}{t_{ki}}\right) - 1 \right] - 2 - \text{Li}_2\left(1 - \frac{\tilde{t}_{kl}}{t_{ki}}\right) \tag{A.15}
\end{aligned}$$

with t_{ki} and \tilde{t}_{kl} defined in (B.3).

A.4 Generic correction factor in the high-energy limit

Using the expressions for the scalar integrals in the high-energy limit given in Appendix B.2, we find

$$\begin{aligned} \Delta_1(k_m, q_j; k_l, q_i) &\sim \frac{1}{2}(s_{ij}\bar{s}_{lm} - \tilde{s}_{lj}\tilde{s}_{mi})D_0(q_j - k_m, q_j + k_l, q_i + q_j, 0, M_m, M_l, 0) \\ &+ \ln\left(\frac{K_m M_l}{K_l M_m}\right) \ln\left(\frac{\tilde{s}_{mi}}{\tilde{s}_{lj}}\right) + \left[2 + \ln\left(\frac{s_{ij}}{\bar{s}_{lm}}\right)\right] \left[\ln\left(\frac{\lambda M_m}{-K_m}\right) + \ln\left(\frac{\lambda M_l}{-K_l}\right)\right] \end{aligned} \quad (\text{A.16})$$

with D_0 defined in (B.30) and

$$\Delta_2(p_k; k_l, q_i) = 2 \ln\left(\frac{\lambda M_l}{-K_l}\right) \left[\ln\left(\frac{\tilde{t}_{kl}}{t_{ki}}\right) - 1\right]. \quad (\text{A.17})$$

Note that we always assume that the resonances decay into a pair of massless particles.

B Scalar integrals for non-factorizable corrections

B.1 Scalar integrals in pole approximation

In Sect. A.2 we have given the virtual non-factorizable corrections in terms of scalar one-loop integrals. In this appendix we list the explicit expressions for these integrals. We have the on-shell conditions for the external particles

$$p_k^2 = (m'_k)^2, \quad q_i^2 = m_i^2, \quad (\text{B.1})$$

and all expression are given for $k_l^2 \rightarrow M_l^2$ and $\Gamma_l \rightarrow 0$, i.e. we neglect $k_l^2 - M_l^2$ and Γ_l everywhere where this does not give rise to singularities. Moreover, we assume

$$(k_l - q_i)^2 = 0, \quad (\text{B.2})$$

which holds if the resonances decay into a pair of massless particles.

We introduce the shorthand notations

$$\begin{aligned} K_l &= k_l^2 - \overline{M}_l^2 \\ t_{ki} &= -2(p_k q_i) = (p_k - q_i)^2, \quad \tilde{t}_{kl} = -2(p_k k_l) \sim (p_k - k_l)^2 - M_l^2, \\ s_{ij} &= 2(q_i q_j) = (q_i + q_j)^2, \quad \tilde{s}_{lj} = 2(k_l q_j) \sim (k_l + q_j)^2 - M_l^2, \\ \bar{s}_{lm} &= 2(k_l k_m) \sim (k_l + k_m)^2 - M_l^2 - M_m^2, \\ w_{lm} &= \sqrt{\lambda[(k_l + k_m)^2, M_l^2, M_m^2]}, \\ r_{lm} &= \frac{1}{2M_l M_m} (-\bar{s}_{lm} + w_{lm}) \left(1 - \frac{i\epsilon}{w_{lm}}\right), \\ \kappa_{lmij} &= \sqrt{\lambda[s_{ij}(\bar{s}_{lm} + s_{ij} - \tilde{s}_{lj} - \tilde{s}_{mi}), (\tilde{s}_{lj} - s_{ij})(\tilde{s}_{mi} - s_{ji}), M_l^2 M_m^2]} \\ &= \sqrt{\lambda[4(q_i q_j)((k_l - q_i)(k_m - q_j)), 4((k_l - q_i)q_j)(q_i(k_m - q_j)), M_l^2 M_m^2]}, \end{aligned} \quad (\text{B.3})$$

where $i\epsilon$ is an infinitesimal imaginary part, and use the definitions

$$\lambda(x, y, z) = x^2 + y^2 + z^2 - 2xy - 2xz - 2yz \quad (\text{B.4})$$

and

$$\begin{aligned} \mathcal{L}i_2(x, y) &= \text{Li}_2(1 - xy) + [\ln(xy) - \ln(x) - \ln(y)] \ln(1 - xy), \\ &|\text{arc}(x)|, |\text{arc}(y)| < \pi \end{aligned} \quad (\text{B.5})$$

with the usual dilogarithm

$$\text{Li}_2(z) = - \int_0^z \frac{dt}{t} \ln(1 - t), \quad |\text{arc}(1 - z)| < \pi. \quad (\text{B.6})$$

The various combinations of scalar integrals read:

case mm

$$\frac{B_0(k_l^2, 0, \overline{M}_l) - B_0(\overline{M}_l^2, 0, \overline{M}_l)}{k_l^2 - \overline{M}_l^2} - B'_0(M_l^2, \lambda, M_l) \sim \frac{1}{M_l^2} \left\{ \ln\left(\frac{\lambda M_l}{-K_l}\right) + 1 \right\}, \quad (\text{B.7})$$

case mf

$$\begin{aligned} C_0(k_l, q_i, 0, \overline{M}_l, m_i) - [C_0(k_l, q_i, \lambda, M_l, m_i)]_{k_l^2=M_l^2} \\ \sim -\frac{1}{M_l^2} \left\{ \ln\left(\frac{m_i^2}{M_l^2}\right) \ln\left(\frac{-K_l}{\lambda M_l}\right) + \ln^2\left(\frac{m_i}{M_l}\right) + \frac{\pi^2}{6} \right\}, \end{aligned} \quad (\text{B.8})$$

case im

$$\begin{aligned} C_0(p_k, k_l, 0, m'_k, \overline{M}_l) - [C_0(p_k, k_l, \lambda, m'_k, M_l)]_{k_l^2=M_l^2} \\ \sim \frac{1}{\tilde{t}_{kl}} \left\{ \ln\left(\frac{m'_k M_l}{-\tilde{t}_{kl}} + i\epsilon\right) \left[\ln\left(\frac{K_l}{\tilde{t}_{kl}}\right) + \ln\left(\frac{-K_l}{\lambda^2}\right) + \ln\left(\frac{m'_k}{M_l}\right) \right] + \frac{\pi^2}{6} \right\}, \end{aligned} \quad (\text{B.9})$$

case mm'

$$\begin{aligned} C_0(k_l, -k_m, 0, \overline{M}_l, \overline{M}_m) - [C_0(k_l, -k_m, \lambda, M_l, M_m)]_{k_l^2=M_l^2, k_m^2=M_m^2} \\ \sim \frac{1}{w_{lm}} \left\{ \mathcal{L}i_2\left(\frac{K_l M_m}{K_m M_l}, \frac{1}{r_{lm}}\right) - \mathcal{L}i_2\left(\frac{K_l M_m}{K_m M_l}, r_{lm}\right) + \mathcal{L}i_2(r_{lm}, r_{lm}) \right. \\ \left. + \ln^2(r_{lm}) + 2 \ln(r_{lm}) \ln\left(\frac{-K_m}{M_m \lambda}\right) \right\}, \end{aligned} \quad (\text{B.10})$$

case if

$$\begin{aligned} D_0(p_k, k_l, q_i, \lambda, m'_k, \overline{M}_l, m_i) \sim -\frac{1}{t_{ki} K_l} \left\{ 2 \ln\left(\frac{-t_{ki}}{m'_k m_i} - i\epsilon\right) \ln\left(\frac{\lambda M_l}{-K_l}\right) \right. \\ \left. + \ln^2\left(\frac{-\tilde{t}_{kl}}{m'_k M_l} - i\epsilon\right) + \ln^2\left(\frac{m_i}{M_l}\right) + \frac{\pi^2}{3} + \text{Li}_2\left(1 - \frac{\tilde{t}_{kl}}{t_{ki}}\right) \right\}, \end{aligned} \quad (\text{B.11})$$

case mf'

$$\begin{aligned}
D_0(1) &= D_0(-q_i, -k_l, k_m, 0, m_i, \overline{M}_l, \overline{M}_m) = D_0(-k_m, k_l, q_i, 0, \overline{M}_m, \overline{M}_l, m_i) \\
&\sim \frac{1}{K_l \tilde{s}_{mi} + K_m M_l^2} \left\{ \sum_{\tau=\pm 1} \left[\mathcal{L}i_2 \left(\frac{K_l M_m}{K_m M_l}, r_{lm}^\tau \right) - \mathcal{L}i_2 \left(-\frac{M_l M_m}{\tilde{s}_{mi}} + i\epsilon, r_{lm}^\tau \right) \right] \right. \\
&\quad - 2 \mathcal{L}i_2 \left(\frac{K_l M_m}{K_m M_l}, -\frac{\tilde{s}_{mi}}{M_l M_m} - i\epsilon \right) \\
&\quad \left. - \ln \left(\frac{m_i^2}{M_l^2} \right) \left[\ln \left(\frac{K_l M_m}{K_m M_l} \right) + \ln \left(-\frac{\tilde{s}_{mi}}{M_l M_m} - i\epsilon \right) \right] \right\}, \tag{B.12}
\end{aligned}$$

case ff'

$$\begin{aligned}
D_0(0) &= D_0(-k_m + q_j, k_l + q_j, q_i + q_j, 0, M_m, M_l, 0) \\
&\sim \frac{1}{\kappa_{lmij}} \sum_{\sigma=1,2} (-1)^\sigma \left\{ \mathcal{L}i_2 \left(-\frac{\tilde{s}_{lj}}{M_l M_m} - i\epsilon, -x_\sigma \right) + \mathcal{L}i_2 \left(-\frac{M_l M_m}{\tilde{s}_{mi}} + i\epsilon, -x_\sigma \right) \right. \\
&\quad \left. - \mathcal{L}i_2 \left(r_{lm}, -x_\sigma \right) - \mathcal{L}i_2 \left(r_{lm}^{-1}, -x_\sigma \right) - \ln \left(\frac{\tilde{s}_{mi}}{s_{ij}} \right) \ln(-x_\sigma) \right\}, \tag{B.13}
\end{aligned}$$

$$\begin{aligned}
\text{with } x_1 &= \frac{(\tilde{s}_{mi} - s_{ji})z}{M_l M_m} - \frac{s_{ij}}{\kappa_{lmij}} i\epsilon, \quad x_2 = \frac{M_l M_m}{(\tilde{s}_{lj} - s_{ij})z} + \frac{s_{ij}}{\kappa_{lmij}} i\epsilon, \\
z &= \frac{M_l^2 M_m^2 + \tilde{s}_{lj} \tilde{s}_{mi} - \bar{s}_{lm} s_{ij} + \kappa_{lmij}}{2(\tilde{s}_{lj} - s_{ij})(\tilde{s}_{mi} - s_{ji})}, \tag{B.14}
\end{aligned}$$

$$\begin{aligned}
D_0(2) &= D_0(-q_j, k_l, q_i, \lambda, m_j, \overline{M}_l, m_i) \\
&\sim -\frac{1}{K_l s_{ij}} \left\{ 2 \ln \left(-\frac{s_{ij}}{m_i m_j} - i\epsilon \right) \ln \left(\frac{\lambda M_l}{-K_l} \right) + \ln^2 \left(-\frac{\tilde{s}_{lj}}{m_j M_l} - i\epsilon \right) \right. \\
&\quad \left. + \ln^2 \left(\frac{m_i}{M_l} \right) + \frac{\pi^2}{3} + \text{Li}_2 \left(1 - \frac{\tilde{s}_{lj}}{s_{ij}} \right) \right\}. \tag{B.15}
\end{aligned}$$

The 5-point function

$$E_0 = E_0(-q_j, -k_m, k_l, q_i, \lambda, m_j, \overline{M}_m, \overline{M}_l, m_i) \tag{B.16}$$

can be reduced to the five 4-point functions

$$\begin{aligned}
D_0(0) &= D_0(-k_m + q_j, k_l + q_j, q_i + q_j, m_j, M_m, M_l, m_i), \\
D_0(1) &= D_0(-k_m, k_l, q_i, 0, \overline{M}_m, \overline{M}_l, m_i), \\
D_0(2) &= D_0(-q_j, k_l, q_i, \lambda, m_j, \overline{M}_l, m_i), \\
D_0(3) &= D_0(-q_j, -k_m, q_i, \lambda, m_j, \overline{M}_m, m_i), \\
D_0(4) &= D_0(-q_j, -k_m, k_l, 0, m_j, \overline{M}_m, \overline{M}_l) \tag{B.17}
\end{aligned}$$

according to

$$E_0 = -\sum_{l=0}^4 \frac{\det(Y_l)}{\det Y} D_0(l). \tag{B.18}$$

The symmetric matrix Y reads (using $\tilde{s}_{li} = M_l^2$)

$$Y = \begin{pmatrix} 0 & 0 & -K_m & -K_l & 0 \\ * & 0 & M_m^2 & (-K_l - \tilde{s}_{lj}) & -s_{ij} \\ * & * & 2M_m^2 & (-\bar{s}_{lm} - K_l - K_m) & (-K_m - \tilde{s}_{mi}) \\ * & * & * & 2M_l^2 & M_l^2 \\ * & * & * & * & 0 \end{pmatrix}, \quad (\text{B.19})$$

and Y_i is obtained from Y by replacing all entries in the i th column with 1.

Neglecting terms that do not contribute to the correction factor in LPA, the corresponding determinants are given by

$$\begin{aligned} \det(Y) &\sim 2s_{ij} \left[K_l K_m (s_{ij} \bar{s}_{lm} - \tilde{s}_{lj} \tilde{s}_{mi}) - M_l^2 M_m^2 \right. \\ &\quad \left. + K_l^2 M_m^2 (s_{ij} - \tilde{s}_{mi}) + K_m^2 M_l^2 (s_{ij} - \tilde{s}_{lj}) \right], \\ \det(Y_0) &\sim \lambda (s_{ij} \bar{s}_{lm}, \tilde{s}_{lj} \tilde{s}_{mi}, M_l^2 M_m^2) + 4s_{ij} M_l^2 M_m^2 (\tilde{s}_{lj} + \tilde{s}_{mi} - s_{ij}), \\ \det(Y_1) &\sim K_l \left[M_l^2 M_m^2 (\tilde{s}_{mi} - 2s_{ij}) + \tilde{s}_{mi} (s_{ij} \bar{s}_{lm} - \tilde{s}_{lj} \tilde{s}_{mi}) \right] \\ &\quad - K_m M_l^2 (s_{ij} \bar{s}_{lm} + \tilde{s}_{lj} \tilde{s}_{mi} - 2s_{ij} \tilde{s}_{mi} - M_l^2 M_m^2), \\ \det(Y_2) &\sim s_{ij} \left[K_l (\tilde{s}_{lj} \tilde{s}_{mi} - s_{ij} \bar{s}_{lm} + M_l^2 M_m^2) + 2K_m M_l^2 (\tilde{s}_{lj} - s_{ij}) \right], \\ \det(Y_3) &= \det(Y_2)|_{i \leftrightarrow j, l \leftrightarrow m}, \\ \det(Y_4) &= \det(Y_1)|_{i \leftrightarrow j, l \leftrightarrow m}. \end{aligned} \quad (\text{B.20})$$

The specific determinants (B.20) appearing in the reduction for the IR-singular E_0 (B.16) with massless external lines obey the relations

$$\begin{aligned} 0 &= \det(Y) + K_m \det(Y_2) + K_l \det(Y_3), \\ 0 &= -\tilde{s}_{mi} \det(Y) + K_m s_{ij} \det(Y_1) - [K_l \tilde{s}_{mi} + K_m M_l^2] \det(Y_3), \\ 0 &= -\tilde{s}_{lj} \det(Y) + K_l s_{ij} \det(Y_4) - [K_m \tilde{s}_{lj} + K_l M_m^2] \det(Y_2). \end{aligned} \quad (\text{B.21})$$

These relations allow us to eliminate $\det(Y_1)$ and $\det(Y_4)$ from (B.18), resulting in:

$$\begin{aligned} E_0(-q_j, -k_m, k_l, q_i, \lambda, m_j, M_m, M_l, m_i) &= -\frac{\det(Y_0)}{\det(Y)} D_0(0) \\ &\quad - \frac{\det(Y_3)}{\det(Y) K_m s_{ij}} \left\{ [K_l \tilde{s}_{mi} + K_m M_l^2] D_0(1) + K_m s_{ij} D_0(3) \right\} \\ &\quad - \frac{\det(Y_2)}{\det(Y) K_l s_{ij}} \left\{ [K_m \tilde{s}_{lj} + K_l M_m^2] D_0(4) + K_l s_{ij} D_0(2) \right\} \\ &\quad - \frac{\tilde{s}_{lj}}{K_l s_{ij}} D_0(4) - \frac{\tilde{s}_{mi}}{K_m s_{ij}} D_0(1). \end{aligned} \quad (\text{B.22})$$

B.2 Scalar integrals in high-energy approximation

In this section we list the integrals with the additional approximation that all invariants are large compared with the masses, i.e.

$$s_{ij}, \tilde{s}_{lj}, \bar{s}_{lm}, t_{ki}, \tilde{t}_{kl} \gg M_l^2. \quad (\text{B.23})$$

We keep only the logarithmic terms and omit also the constant terms.

The various combinations of scalar integrals read:

case mm

$$\frac{B_0(k_l^2, 0, \overline{M}_l) - B_0(\overline{M}_l^2, 0, \overline{M}_l)}{k_l^2 - \overline{M}_l^2} - B'_0(M_l^2, \lambda, M_l) \sim \frac{1}{M_l^2} \ln\left(\frac{\lambda M_l}{-K_l}\right), \quad (\text{B.24})$$

case mf

$$\begin{aligned} & C_0(k_l, q_i, 0, \overline{M}_l, m_i) - \left[C_0(k_l, q_i, \lambda, M_l, m_i) \right]_{k_l^2=M_l^2} \\ & \sim -\frac{1}{M_l^2} \ln\left(\frac{m_i}{M_l}\right) \left[2 \ln\left(\frac{-K_l}{\lambda M_l}\right) + \ln\left(\frac{m_i}{M_l}\right) \right], \end{aligned} \quad (\text{B.25})$$

case im

$$\begin{aligned} & C_0(p_k, k_l, 0, m'_k, \overline{M}_l) - \left[C_0(p_k, k_l, \lambda, m'_k, M_l) \right]_{k_l^2=M_l^2} \\ & \sim \frac{1}{\tilde{t}_{kl}} \ln\left(\frac{m'_k M_l}{-\tilde{t}_{kl}} + i\epsilon\right) \left[\ln\left(\frac{K_l}{\tilde{t}_{kl}}\right) + \ln\left(\frac{-K_l}{\lambda^2}\right) + \ln\left(\frac{m'_k}{M_l}\right) \right], \end{aligned} \quad (\text{B.26})$$

case mm'

$$\begin{aligned} & C_0(k_l, -k_m, 0, \overline{M}_l, \overline{M}_m) - \left[C_0(k_l, -k_m, \lambda, M_l, M_m) \right]_{k_l^2=M_l^2, k_m^2=M_m^2} \\ & \sim \frac{1}{\bar{s}_{lm}} \left\{ \ln\left(\frac{M_l M_m}{-\bar{s}_{lm}} + i\epsilon\right) \ln\left(\frac{-\bar{s}_{lm}}{\lambda^2} - i\epsilon\right) + \ln\left(\frac{\bar{s}_{lm}}{K_l}\right) \ln\left(\frac{\bar{s}_{lm}}{K_m}\right) - \frac{1}{2} \ln^2\left(\frac{M_l^2}{-K_l}\right) \right. \\ & \quad \left. - \frac{1}{2} \ln^2\left(\frac{M_m^2}{-K_m}\right) + \frac{1}{4} \ln^2\left(\frac{-\bar{s}_{lm}}{M_l^2} - i\epsilon\right) + \frac{1}{4} \ln^2\left(\frac{-\bar{s}_{lm}}{M_m^2} - i\epsilon\right) \right\}, \end{aligned} \quad (\text{B.27})$$

case if

$$\begin{aligned} & D_0(p_k, k_l, q_i, \lambda, m'_k, \overline{M}_l, m_i) \\ & \sim -\frac{1}{t_{ki} K_l} \left\{ 2 \ln\left(\frac{-t_{ki}}{m'_k m_i} - i\epsilon\right) \ln\left(\frac{\lambda M_l}{-K_l}\right) + \ln^2\left(\frac{-t_{ki}}{m'_k m_i} - i\epsilon\right) + \ln^2\left(\frac{m_i}{M_l}\right) \right\}, \end{aligned} \quad (\text{B.28})$$

case mf'

$$\begin{aligned} & D_0(1) = D_0(-q_i, -k_l, k_m, 0, m_i, \overline{M}_l, \overline{M}_m) \\ & \sim \frac{1}{K_l \tilde{s}_{mi}} \left\{ \ln^2\left(\frac{-\tilde{s}_{mi}}{M_l^2} - i\epsilon\right) - \frac{1}{2} \ln^2\left(\frac{-\bar{s}_{lm}}{M_l^2} - i\epsilon\right) - \ln\left(\frac{-\tilde{s}_{mi}}{M_l^2} - i\epsilon\right) \ln\left(\frac{m_i^2}{M_l^2}\right) \right. \\ & \quad \left. + \frac{1}{2} \ln^2\left(\frac{K_l}{K_m}\right) + \ln\left(\frac{K_l}{K_m}\right) \left[\ln\left(\frac{-\tilde{s}_{mi}}{m_i^2} - i\epsilon\right) + \ln\left(\frac{\tilde{s}_{mi} + i\epsilon}{\bar{s}_{lm} + i\epsilon}\right) \right] \right\}, \end{aligned} \quad (\text{B.29})$$

case ff'

$$\begin{aligned}
D_0(0) &= D_0(-k_m + q_j, k_l + q_j, q_i + q_j, 0, M_m, M_l, 0) \\
&\sim -\frac{1}{\tilde{s}_{lj}\tilde{s}_{mi} - \bar{s}_{lm}s_{ij}} \left\{ \mathcal{L}i_2\left(-\frac{M_l M_m}{\tilde{s}_{mi}} + i\epsilon, -x_1\right) + \mathcal{L}i_2\left(-\frac{M_l M_m}{\tilde{s}_{lj}} + i\epsilon, -\frac{1}{x_2}\right) \right. \\
&\quad - \mathcal{L}i_2\left(-\frac{M_l M_m}{\bar{s}_{lm}} + i\epsilon, -x_1\right) - \mathcal{L}i_2\left(-\frac{M_l M_m}{\bar{s}_{lm}} + i\epsilon, -\frac{1}{x_2}\right) \\
&\quad \left. - \left[\ln\left(\frac{\tilde{s}_{mi} + i\epsilon}{s_{ij} + i\epsilon}\right) + \ln\left(\frac{\tilde{s}_{lj} + i\epsilon}{\bar{s}_{lm} + i\epsilon}\right) \right] (\ln(-x_1) - \ln(-x_2)) \right\} \quad (B.30)
\end{aligned}$$

$$\begin{aligned}
\text{with } x_1 &= \frac{(\tilde{s}_{mi} - s_{ij})z}{M_l M_m} (1 - i\epsilon s_{ij}(\tilde{s}_{lj} - s_{ij})), \\
x_2 &= \frac{M_l M_m}{(\tilde{s}_{lj} - s_{ij})z} (1 + i\epsilon s_{ij}(\tilde{s}_{mi} - s_{ij})), \\
z &= \frac{\tilde{s}_{lj}\tilde{s}_{mi} - \bar{s}_{lm}s_{ij}}{(\tilde{s}_{lj} - s_{ij})(\tilde{s}_{mi} - s_{ij})}, \quad (B.31)
\end{aligned}$$

$$\begin{aligned}
D_0(2) &= D_0(-q_j, k_l, q_i, \lambda, m_j, \bar{M}_l, m_i) \\
&\sim -\frac{1}{K_l s_{ij}} \left\{ 2 \ln\left(-\frac{s_{ij}}{m_i m_j} - i\epsilon\right) \ln\left(\frac{\lambda M_l}{-K_l}\right) + \ln^2\left(-\frac{\tilde{s}_{lj}}{m_j M_l} - i\epsilon\right) + \ln^2\left(\frac{m_i}{M_l}\right) \right\}. \quad (B.32)
\end{aligned}$$

We note that $D_0(0)$ does not involve large logarithms and could be replaced by zero in the logarithmic approximation.

C Couplings

In this appendix we list the explicit values for the couplings $I_{\phi_i \phi_{i'}}^V$ introduced in Ref. [18] required for our calculation. Note that a bar over a field indicates the charge-conjugated field.

For quarks the couplings $I_{q_i, \sigma q_j, \sigma}^V$ depend on the helicity σ and involve the quark-mixing matrix V_{ij} :

$$\begin{aligned}
I_{q-q-}^A &= I_{q+q+}^A = -Q_q, \\
I_{q-q-}^Z &= \frac{I_q^3 - s_w^2 Q_q}{s_w c_w}, \quad I_{q+q+}^Z = -\frac{s_w Q_q}{c_w}, \\
I_{u_i, -d_j, -}^{W^+} &= \frac{1}{\sqrt{2} s_w} V_{ij}, \quad I_{d_j, -u_i, -}^{W^-} = \frac{1}{\sqrt{2} s_w} V_{ij}^*. \quad (C.1)
\end{aligned}$$

All other quark couplings vanish, and the couplings for antiquarks are obtained by

$$I_{\bar{q}_i, \sigma \bar{q}_j, \sigma}^V = -I_{q_j, -\sigma q_i, -\sigma}^V. \quad (C.2)$$

For gauge bosons the couplings $I_{V_2 V_3}^{V_1}$ are totally antisymmetric in the field indices V_1, V_2, V_3 and read

$$I_{W^- W^-}^A = I_{W^+ A}^{W^+} = I_{AW^+}^{W^-} = -I_{W^+ W^+}^A = -I_{W^- A}^{W^-} = -I_{AW^-}^{W^+} = 1,$$

$$I_{W^-W^-}^Z = I_{W^+Z}^{W^+} = I_{ZW^+}^{W^-} = -I_{W^+W^+}^Z = -I_{W^-Z}^{W^-} = -I_{ZW^-}^{W^+} = -\frac{c_w}{s_w}. \quad (\text{C.3})$$

For Higgs and would-be Goldstone bosons, the couplings $I_{S_1 S_2}^V$ are antisymmetric in the scalar fields S_1 and S_2 and read

$$\begin{aligned} I_{\chi H}^Z &= -I_{H\chi}^Z = \frac{i}{2c_w s_w}, \\ I_{\phi^-\phi^-}^A &= -I_{\phi^+\phi^+}^A = 1, \quad I_{\phi^-\phi^-}^Z = -I_{\phi^+\phi^+}^Z = -\frac{c_w^2 - s_w^2}{2c_w s_w}, \\ I_{\phi^\pm H}^{W^\pm} &= -I_{H\phi^\mp}^{W^\pm} = \pm \frac{1}{2s_w}, \quad I_{\phi^\pm\chi}^{W^\pm} = -I_{\chi\phi^\mp}^{W^\pm} = \frac{i}{2s_w}. \end{aligned} \quad (\text{C.4})$$

The couplings appearing in the lowest-order matrix elements for four-fermion production can be read off from Appendix A of Ref. [27] and are related to the quantities $I_{ff'}^V$ via

$$C_{V\bar{f}f'}^{\sigma\sigma'} = \delta_{\sigma,-\sigma'} I_{f_{\sigma'} f_{\sigma}}^V. \quad (\text{C.5})$$

References

- [1] S. Haywood *et al.*, hep-ph/0003275, in *Standard Model Physics (and more) at the LHC*, eds. G. Altarelli and M. L. Mangano, (CERN-2000-004, Genève, 2000) p. 117 [hep-ph/0003275] and references therein.
- [2] B. Mele, P. Nason and G. Ridolfi, Nucl. Phys. B **357** (1991) 409;
J. Ohnemus and J. F. Owens, Phys. Rev. D **43** (1991) 3626;
J. Ohnemus, Phys. Rev. D **44** (1991) 1403;
S. Frixione, Nucl. Phys. B **410** (1993) 280;
J. Ohnemus, Phys. Rev. D **44** (1991) 3477.
- [3] S. Frixione, P. Nason and G. Ridolfi, Nucl. Phys. B **383** (1992) 3.
- [4] J. Ohnemus, Phys. Rev. D **50** (1994) 1931 [hep-ph/9403331].
- [5] U. Baur, T. Han and J. Ohnemus, Phys. Rev. D **53** (1996) 1098 [hep-ph/9507336].
- [6] U. Baur, T. Han and J. Ohnemus, Phys. Rev. D **51** (1995) 3381 [hep-ph/9410266].
- [7] L. Dixon, Z. Kunszt and A. Signer, Phys. Rev. D **60** (1999) 114037 [hep-ph/9907305].
- [8] J. M. Campbell and R. K. Ellis, Phys. Rev. D **60** (1999) 113006 [hep-ph/9905386].
- [9] U. Baur, S. Keller and D. Wackerth, Phys. Rev. D **59** (1999) 013002 [hep-ph/9807417];
U. Baur *et al.*, Phys. Rev. D **65** (2002) 033007 [hep-ph/0108274];
S. Dittmaier and M. Krämer, Phys. Rev. D **65** (2002) 073007 [hep-ph/0109062];
U. Baur and D. Wackerth, hep-ph/0405191.
- [10] W. Beenakker *et al.*, Nucl. Phys. B **411** (1994) 343.

- [11] E. Maina *et al.*, Phys. Lett. B **570** (2003) 205 [hep-ph/0307021].
- [12] E. Maina, S. Moretti and D. A. Ross, hep-ph/0403050;
J. H. Kühn *et al.*, hep-ph/0408308.
- [13] M. L. Ciccolini, S. Dittmaier and M. Krämer, Phys. Rev. D **68** (2003) 073003 [hep-ph/0306234].
- [14] W. Hollik and C. Meier, Phys. Lett. B **590** (2004) 69 [arXiv:hep-ph/0402281].
- [15] E. Accomando, A. Denner and S. Pozzorini, Phys. Rev. D **65** (2002) 073003 [hep-ph/0110114].
- [16] W. Beenakker *et al.*, Nucl. Phys. B **410** (1993) 245.
- [17] P. Ciafaloni and D. Comelli, Phys. Lett. B **446** (1999) 278 [hep-ph/9809321];
M. Beccaria *et al.*, Phys. Rev. D **61** (2000) 073005 [hep-ph/9906319];
V. S. Fadin *et al.*, Phys. Rev. D **61** (2000) 094002 [hep-ph/9910338];
W. Beenakker and A. Werthenbach, Phys. Lett. B **489** (2000) 148 [hep-ph/0005316];
Nucl. Phys. B **630** (2002) 3 [hep-ph/0112030];
J. Layssac and F. M. Renard, Phys. Rev. D **64** (2001) 053018 [hep-ph/0104205];
M. Melles, Phys. Rept. **375** (2003) 219 [hep-ph/0104232];
J. H. Kühn *et al.*, Nucl. Phys. B **616** (2001) 286 [Erratum-ibid. B **648** (2003) 455] [hep-ph/0106298];
M. Beccaria, F. M. Renard and C. Verzegnassi, Nucl. Phys. B **663** (2003) 394 [hep-ph/0304175];
S. Pozzorini, Nucl. Phys. B **692** (2004) 135 [hep-ph/0401087];
B. Feucht, J. H. Kühn, A. A. Penin and V. A. Smirnov, hep-ph/0404082.
- [18] A. Denner and S. Pozzorini, Eur. Phys. J. C **18** (2001) 461 [hep-ph/0010201].
- [19] A. Denner and S. Pozzorini, Eur. Phys. J. C **21** (2001) 63 [hep-ph/0104127].
- [20] S. Pozzorini, *Dissertation, University of Zurich*, 2001, hep-ph/0201077.
- [21] F. Abe *et al.* (CDF Collaboration), Phys. Rev. Lett. **75** (1995) 1017;
F. Abachi *et al.* (D0 Collaboration), Phys. Rev. Lett. **77** (1996) 3301; Phys. Rev. Lett. **79** (1997) 1441.
- [22] A. Denner *et al.*, Nucl. Phys. B **587** (2000) 67 [hep-ph/0006307].
- [23] A. Denner *et al.*, Nucl. Phys. B **560** (1999) 33 [hep-ph/9904472].
- [24] A. Kaiser, *Dissertation, University of Zurich*, 2004.
- [25] F. A. Berends *et al.*, Nucl. Phys. B **206** (1982) 61;
R. Kleiss, Z. Phys. C **33** (1987) 433.
- [26] D. R. Yennie, S. C. Frautschi and H. Suura, Annals Phys. **13** (1961) 379.

- [27] A. Denner, Fortsch. Phys. **41** (1993) 307.
- [28] G. 't Hooft and M. J. G. Veltman, Nucl. Phys. B **153** (1979) 365.
- [29] J. Kripfganz and H. Perlt, Z. Phys. C **41** (1988) 319;
H. Spiesberger, Phys. Rev. D **52** (1995) 4936 [hep-ph/9412286];
M. Roth and S. Weinzierl, Phys. Lett. B **590** (2004) 190 [hep-ph/0403200].
- [30] K. Hagiwara *et al.* [Particle Data Group Collaboration], Phys. Rev. D **66** (2002) 010001.
- [31] The CDF Collaboration, the D0 Collaboration, the Tevatron Electroweak Working Group, hep-ex/0404010.
- [32] A. Höcker *et al.*, Eur. Phys. J. C **21** (2001) 225 [hep-ph/0104062].
- [33] J. Pumplin *et al.*, JHEP 0207 (2002) 012 [hep-ph/0201195].
- [34] U. Baur, T. Han and J. Ohnemus, Phys. Rev. Lett. **72** (1994) 3941 [hep-ph/9403248].
- [35] G. J. Gounaris, J. Layssac and F. M. Renard, Phys. Rev. D **62** (2000) 073013 [hep-ph/0003143];
G. J. Gounaris, J. Layssac and F. M. Renard, Phys. Rev. D **61** (2000) 073013 [hep-ph/9910395];
D. Choudhury *et al.*, Int. J. Mod. Phys. A **16** (2001) 4891 [hep-ph/0011205].
- [36] U. Baur and E. L. Berger, Phys. Rev. D **47** (1993) 4889;
U. Baur, T. Han and J. Ohnemus, Phys. Rev. D **57** (1998) 2823 [hep-ph/9710416].
- [37] A. Denner, S. Dittmaier and M. Roth, Nucl. Phys. B **519** (1998) 39 [hep-ph/9710521].
- [38] A. Aeppli, G. J. van Oldenborgh and D. Wyler, Nucl. Phys. B **428** (1994) 126 [hep-ph/9312212].
- [39] W. Beenakker, A. P. Chapovsky and F. A. Berends, Phys. Lett. B **411** (1997) 203 [hep-ph/9706339]; Nucl. Phys. B **508** (1997) 17 [hep-ph/9707326].